A thermal pressurization model for the spontaneous dynamic rupture propagation on a three-dimensional fault: 1. Methodological approach

A. Bizzarri[1,2] and M. Cocco[1]

Received 3 June 2005; revised 16 December 2005; accepted 30 January 2006; published 2 May 2006.

[1] We investigate the role of frictional heating and thermal pressurization on earthquake ruptures by modeling the spontaneous propagation of a three-dimensional (3-D) crack on a planar fault governed by assigned constitutive laws and allowing the evolution of effective normal stress. We use both slip-weakening and rate- and state-dependent constitutive laws; in this latter case we employ the Linker and Dieterich evolution law for the state variable, and we couple the temporal variations of friction coefficient with those of effective normal stress. In the companion paper we investigate the effects of thermal pressurization on the dynamic traction evolution. We solve the 1-D heat conduction equation coupled with Darcy's law for fluid flow in porous media. We obtain a relation that couples pore fluid pressure to the temperature evolution on the fault plane. We analytically solve the thermal pressurization problem by considering an appropriate heat source for a fault of finite thickness. Our modeling results show that thermal pressurization reduces the temperature increase caused by frictional heating. However, the effect of the slipping zone thickness on temperature changes is stronger than that of thermal pressurization, at least for a constant porosity model. Pore pressure and effective normal stress evolution affect the dynamic propagation of the earthquake rupture producing a shorter breakdown time and larger breakdown stress drop and rupture velocity. The evolution of the state variable in the framework of rate- and state-dependent friction laws is very different when thermal pressurization is active. In this case the evolution of the friction coefficient differs substantially from that inferred from a slip-weakening law. This implies that the traction evolution and the dynamic parameters are strongly affected by thermal pressurization.

Citation: Bizzarri, A., and M. Cocco (2006), A thermal pressurization model for the spontaneous dynamic rupture propagation on a three-dimensional fault: 1. Methodological approach, *J. Geophys. Res.*, *111*, B05303, doi:10.1029/2005JB003862.

1. Introduction

[2] The role of fluids and pore pressure relaxation on the mechanics of earthquakes and faulting has been the object of a large number of studies, based both on observations and on theoretical modeling. Ample evidence have been discussed to demonstrate that fluid flow and/or pore pressure evolution can affect earthquake ruptures. *Hubbert and Rubey* [1959] emphasized the importance of fluid pressure for the effective normal stress, in particular when the fault mechanical conditions are moved from a hydrostatic regime ($So \cong 0.4$) to a lithostatic one ($So \cong 1$, where So is the dimensionless Sommerfeld number [*Sommerfeld*, 1950] that is the ratio between the fluid pressure, p_{fluid}, and the normal stress σ_n). Fluids can affect the earthquake nucleation process: high fluid pressure can allow fault reactivation with the inversion of slip direction (such as low angle thrust fault reactivated by normal faulting [see *Sibson*, 1986; *Collettini et al.*, 2005, and references therein]). They can also trigger aftershocks controlling the patterns of seismicity both in space and time [e.g., *Nur and Booker*, 1972; *Miller et al.*, 1996, 2004; *Yamashita*, 1998; *Shapiro et al.*, 2003; *Antonioli et al.*, 2006]. Fluid flow and pore pressure evolution can also affect the dynamic propagation of earthquake ruptures: frictional heating caused by earthquake dislocation can modify the pore pressure and therefore the effective normal stress acting on the fault surface. This process, called thermal pressurization, has been proposed in the literature long ago [*Sibson*, 1973; *Lachenbruch*, 1980; *Raleigh and Everden*, 1981; *Mase and Smith*, 1985, 1987] and more recently by *Andrews* [2002]. Other authors [e.g., *Irwin and Barnes*, 1975; *Rudnicki and Chen*, 1988; *Byerlee*, 1990; *Rice*, 1992; *Lockner and Byerlee*, 1995] proposed various physical mechanisms that are able to maintain high fluid pressure in fault zones. Despite the numerous papers in the literature, the presence and the role of fluids on dynamic fault weakening is still a matter of debate within the scientific community. More recently, *Kanamori and Heaton* [2000] emphasized again that during large earthquakes the

[1]Istituto Nazionale di Geofisica e Vulcanologia, Sezione di Sismologia e Tettonofisica, Rome, Italy.
[2]Now at the Istituto Nazionale di Geofisica e Vulcanologia, Sezione di Bologna, Bologna, Italy.

0148-0227/06/2005JB003862$09.00

thermal pressurization phenomenon is important. In this work we aim to discuss the role of thermal pressurization on earthquake ruptures by modeling the spontaneous propagation of a three-dimensional (3-D) rupture governed by assigned constitutive laws allowing the evolution of effective normal stress ($\sigma_n^{\text{eff}} = \sigma_n - p_{\text{fluid}}$).

[3] The increase of temperature caused by dynamic slip episodes during earthquake ruptures is usually named frictional heating [see, e.g., *Fialko*, 2004, and references therein]. The temperature changes in a poroelastic medium modify pore pressure, leading to temporal variations of the effective normal stress acting on the fault surface. This is the basic idea we follow in constructing our numerical experiments that we discuss in this study. Although we limit our study to coseismic processes, it is important to remember here that pore pressure can also change during the interseismic period due to compaction and sealing of fault zones [*Blanpied et al.*, 1992; *Sleep and Blanpied*, 1992]. *Sibson* [2003] presents a comprehensive discussion on the structure and the thickness of the slipping zone, pointing out the role of frictional heating to induce partial melting of fault gouge. He emphasizes that one meter of slip on a slipping zone few millimeters thick would produce temperature changes larger than 1000 °C under adiabatic conditions (i.e., with no exchange of heat), and therefore cause melting of most crustal rocks [see also *Fialko*, 2004]. *Sibson* [2003] raises an interesting question related to the apparent scarcity of pseudotachylyte and the common evidence of slip localization in fault zones, suggesting that this might be explained either if friction melting is a rare phenomenon or if pseudotachylyte, created at depth, is not preserved in exhumed fault zones. Melting has been also observed in laboratory experiments [*Friedman et al.*, 1974; *Teufel and Logan*, 1979; *Tsutsumi and Shimamoto*, 1997]. If melts have a very low viscosity they may lubricate faults [*Spray*, 1993; *Fialko*, 2004] and cause rapid changes in friction. Several mechanisms have been proposed in the literature to explain this sudden drop of the friction coefficient and the associated dynamic fault weakening; they include melting [*Jeffreys*, 1942; *McKenzie and Brune*, 1972; *Richards*, 1976; *Cardwell et al.*, 1978; *Sibson*, 1977; *Allen*, 1979], acoustic fluidization [*Melosh*, 1979, 1996] and mechanical lubrication [*Spray*, 1993; *Brodsky and Kanamori*, 2001; *Kanamori and Brodsky*, 2001]. Melting of gouge materials can also arrest the dynamic rupture by viscous braking, as also observed in laboratory experiments by *Tsutsumi and Shimamoto* [1997]. This may happen when an uninterrupted layer of melt with a relatively high viscosity is formed along the fault surface; in such conditions viscous deformation controls the resistance to slip and not the usual Terzaghi or Mohr-Coulomb law [*Fialko*, 2004].

[4] Because in our study we use different constitutive laws to model the spontaneous propagation of an earthquake rupture, we have to account for the temporal changes of effective normal stress caused by thermal pressurization in the analytical formulation of the friction law. To this end, we consider the temporal changes of effective normal stress in the analytical expression of fault friction and, in the case of rate- and state-dependent laws [e.g., *Dieterich*, 1978, 1986, 1994; *Ruina*, 1980, 1983], also in the evolution of the state variable [*Linker and Dieterich*, 1992] as we discuss in sections 3 and 6. In the literature, there are many papers describing laboratory experiments involving normal stress variations and related phenomena. *Linker and Dieterich* [1992] and *Dieterich and Linker* [1992] show the effects of imposed step variations in normal stress on fault friction: a sudden change in normal stress produces a direct response on friction and an evolving relaxation to a new steady state, analogously to a sudden change in load point velocity. More recently, *Prakash* [1998] examined the frictional response due to temporally varying imposed normal stress. *Richardson and Marone* [1999] presented experimental results about effects on frictional healing of normal stress vibrations.

[5] A thermal pressurization model requires assignment of the permeability and the porosity of the medium [see *Andrews*, 2002, and references therein]. In most of the applications, porosity is considered to be constant. However, several authors have investigated the porosity evolution: *Segall and Rice* [1995] propose different analytical relations to describe the porosity change due to frictional dilatancy and ductile compaction, although they did not consider frictional heating. *Sleep* [1995a, 1995b, 1997, 1999] and *Sleep et al.* [2000] propose different analytical relations to account for ductile creep, compaction and other conditions that can modify the porosity. A recent work of *Andrews* [2002] is focused on the effects of fluid pressure changes due to frictional heating in a 3-D fault model governed by a time-weakening (TW) friction law, in which the hydraulic diffusivity is assumed to be constant and the porosity obeys to Biot's theory of saturated porous media.

[6] In spite of the profusion of experimental and theoretical works, there are no numerical simulations that consider a realistic fault model and that include all these physical phenomena. *Miller* [2002], using the model of *Segall and Rice* [1995], and therefore neglecting thermal effects, modeled the influence of fluids on earthquake and faulting, assuming the radiation damping approximation (RDA [see, e.g., *Rice*, 1993]) and a simple constitutive law with two levels of friction. *Perfettini et al.* [2003], still adopting the RDA, modeled the effects of externally imposed analytical variations in normal stress and their effects on a fault obeying to the *Linker and Dieterich* [1992] constitutive equation.

[7] The aim of the present work is to discuss the influence of thermal pressurization on dynamic earthquake ruptures by performing several numerical experiments using different constitutive laws and a constant porosity. In the companion paper by *Bizzarri and Cocco* [2006] (hereinafter referred to as BC06) we present the effect of thermal pressurization on the dynamic traction evolution, and we consider the effects of temporal porosity changes. In the present study we focus on the temperature variations caused by thermal pressurization as well as on the effective normal stress changes affecting the evolution of the friction coefficient.

2. Simulation Strategy

[8] In this paper we model the fully dynamic spontaneous propagation of an earthquake rupture on a vertical strike-slip fault in a homogeneous half-space by solving the elastodynamic fundamental equation, neglecting body forces, using the truly 3-D, second-order in space and in time, Finite Difference conventional grid based code presented by *Bizzarri and Cocco* [2005]. We refer the reader to that paper for all the details and for the analysis of convergence and stability.

[9] The solution of this problem requires the adoption of a governing law to model fault friction, which is necessary to have a finite fracture energy absorbed at the crack tip. The implementation of such a fault boundary condition (FBC) is done by using the traction-at-split-nodes (TSN) technique, proposed in 3-D by *Day* [1977], *Archuleta and Day* [1980], *Day* [1982a, 1982b] and *Andrews* [1999], which allows the calculation of all components of traction and slip at the same fault position.

[10] The shear traction degradation for increasing slip during the dynamic rupture propagation is controlled by the adopted constitutive law. This allows us to define the spatial extension of the cohesive (or breakdown) zone as well as the duration of the breakdown process (i.e., the duration of the decrease of the fault friction from the upper yield value down to the kinetic residual level). In this study and in BC06 we refer to the breakdown processes as the physical mechanisms controlling the shear stress degradation within the cohesive zone at the crack tip. The FBC on the fault surface is represented by either slip weakening or rate- and state-dependent friction laws, which are briefly described in section 3.

[11] Because in this study we are interested in modeling the dynamic rupture propagation, earthquake nucleation is promoted and modeled either by means of time weakening or by an appropriate state variable configuration in a predetermined nucleation patch, as explained in detail for the 2-D case by *Bizzarri et al.* [2001] and for the 3-D one by *Bizzarri and Cocco* [2005]. Thus, in our modeling strategy the latest stages of rupture nucleation and the dynamic rupture onset are controlled by the adopted constitutive law. All numerical results are evaluated at points located far enough from the hypocenter to be completely unaffected by the nucleation processes.

[12] We consider the effect of temperature increase caused by frictional heating. Once slip starts to accelerate and slip velocity increases, temperature changes due to frictional heating. The temperature increase modifies the pore fluid pressure, which in turn changes the modulus of the effective normal traction according to the Terzaghi effective stress law [*Terzaghi et al.*, 1996; *Wang*, 2000]: $\sigma_n^{\text{eff}} = \sigma_n - p_{\text{fluid}}$, where σ_n is the value of the normal stress and p_{fluid} is the value of the pore fluid pressure. The modulus τ of the shear traction is related to σ_n^{eff} through the well known relation: $\tau = \mu\sigma_n^{\text{eff}}$, μ being the friction coefficient. Therefore we aim to model the shear traction evolution by means of the temporal variations of both the friction coefficient and the effective normal stress. In other words, we aim to simulate the effects of thermal pressurization of pore fluids on the earthquake rupture propagation. In this context, the adopted constitutive law controls the traction evolution at low slip rates, while at large slip velocities it is mainly controlled by thermal pressurization caused by frictional heating. This issue is discussed in detail in BC06. Our simulations differ from those presented by *Fialko* [2004] with a 2-D model because we account for the spontaneous evolution of the breakdown process in the cohesive zone (governed by the constitutive law). They also differ from those presented by *Andrews* [2002] since we include different constitutive laws and we consider in the analytical solution for temperature and pore pressure evolutions proper elementary solutions and an appropriate heat source for a fault of finite thickness. Moreover, we do not introduce any artificial fading memory in the value of the effective normal stress: in this study we implicitly assume that changes in normal stress produce variations in shear strength on the same timescale. The use of a sudden time evolution of σ_n^{eff} is also consistent with the experimental results of *Prakash* [1998], who showed that the delayed temporal response of shear stress due to a change in normal stress is less than few microseconds.

[13] We consider a fault model consisting of a narrow zone having a prescribed thickness ($2w$) where the slip is localized, and we refer to this as the slipping zone (see Figure 1). The shear stress, slip and slip velocity used in the constitutive formulation should be considered as macroscopic averages of complex processes occurring within the slipping zone (asperity fractures, gouge formation and evolution, etc.). In other words, we should regard these physical quantities as macroscopic variables [*Ohnaka*, 2003]. Frictional heating is generated within the slipping zone and the rate of frictional heat generation depends on the macroscopic frictional slip rate and the total dynamic traction; the heat rate is inversely proportional to the thickness ($2w$) of the slipping zone [see *Fialko*, 2004, and references therein]. If the thickness of the slipping zone (i.e., the gouge layer) is constant along the rupture plane and the shear strain rate ($\dot{e}$) is uniform across the slipping zone, then slip rate (v) and strain rate scale through the thickness $2w$ ($v = 2w\dot{e}$ [see *Sleep et al.*, 2000]). In this case, we can consider the macroscopic slip rate as well as the dynamic traction and the slip acting on both walls of the slipping zone as the main physical quantities characterizing the constitutive laws. In order to perform our numerical calculations, in this study we compute the temperature, friction and effective normal stress changes on a specified fault plane and we implicitly assume that they are representative of the macroscopic behavior of the whole slipping zone. The effective normal stress is altered by the thermally induced pore pressure changes occurring perpendicularly to the fault plane as we discuss in detail in sections 4.2 and 6.

[14] In reality, it is common to consider that the slipping zone is embedded within a highly fractured damage zone (see Figure 1a and *Chester et al.* [1993] and *Sibson* [2003]) characterized by a higher permeability than the fault core. However, in this study we use a simpler configuration than that shown in Figure 1a, and we represent the damage zone as a homogeneous and isotropic medium. Because we aim to solve a thermal pressurization problem, we have to assign several parameters in the 3-D medium, such as thermal diffusivity, porosity and permeability. In this work we take these values constant throughout the medium (see Figure 1b). The modeling of spatial and temporal variations of permeability is beyond the goals of the present study. This is because there exist serious difficulties in constraining the temporal evolution of permeability within the fault and the damage zones caused by shear dislocations. This topic will be considered in future research. In sections 5 and 6 we describe the analytical solution of the problem and we discuss the constitutive laws governing fault friction.

3. Modeling the Breakdown Processes

[15] As mentioned above, in this study we use both slip weakening (SW) and rate- and state-dependent constitutive

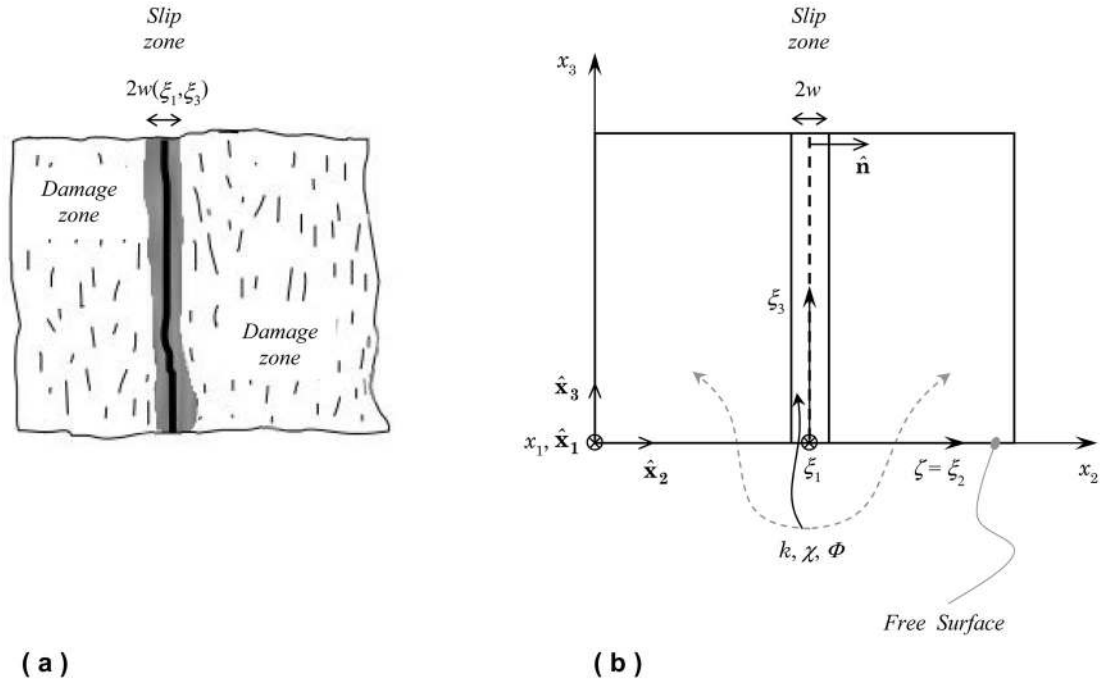

Figure 1. (a) Fault zone structure inferred from geological observations [e.g., *Chester et al.*, 1993; *Chester and Chester*, 1998; *Lockner et al.*, 2000; *Wibberley and Shimamoto*, 2003; *Sibson*, 2003]. The slipping region has a thickness $2w$, and it is indicated by the shaded area; the solid line is the principal slipping zone [*Sibson*, 2003]. The fault core in embedded in a highly fractured damage zone [*Li et al.*, 1994]. (b) The fault model used in this work. The $2w$ represents the thickness of the slipping zone, and the straight line in the center is the fault plane ($\zeta = 0$). The permeability (k), porosity (Φ), and thermal diffusivity (χ) are taken constant through the medium. $Ox_1x_2x_3$ is the absolute Cartesian coordinate system, while $O\xi_1\zeta\xi_3$ is the local one.

relations (RS). The former is represented by the linear relation between total traction and fault slip [*Ida*, 1972; *Andrews*, 1976a, 1976b]:

$$\tau = \begin{cases} \tau_u - (\tau_u - \tau_f)\dfrac{u}{d_0}, & u < d_0 \\ \tau_f, & u \geq d_0 \end{cases} \tag{1}$$

where u is the fault slip, τ_u is the upper yield stress (i.e., the maximum value that the rock can endure), τ_f the kinetic (or residual) frictional level and d_0 is the characteristic SW distance. The difference existing between τ_u and τ_f defines the breakdown stress drop ($\Delta\tau_b$). The two frictional parameters appearing in (1) can be written as $\tau_u = \mu_u\sigma_n^{\text{eff}}$ and $\tau_f = \mu_f\sigma_n^{\text{eff}}$ (where μ_u and μ_f are the static and dynamic coefficient of friction, respectively), and therefore they explicitly depend on the pore pressure value.

[16] Rate- and state-dependent constitutive relations have been used to model the fully dynamic spontaneous rupture propagation both in two dimensions [*Okubo*, 1989; *Bizzarri and Cocco*, 2003, and references therein] and in a truly 3-D fault models [see *Bizzarri and Cocco*, 2005]. These constitutive laws have been derived from the results of laboratory experiments [e.g., *Dieterich*, 1978; *Ruina*, 1980, 1983; *Beeler et al.*, 1994; *Roy and Marone*, 1996; *Marone*, 1998] performed at low slip rates (<1 mm/s) and constant normal stress. The analytical formulation of these constitutive laws consists of two equations: a governing equation, which relates total traction to slip velocity and the state variable, and an evolution equation for the state variable. It is well known, however, that the assumption of a constant normal stress is not always appropriate to model real faulting episodes. Previous investigations [*Hobbs and Brady*, 1985; *Lockner et al.*, 1986; *Olsson*, 1988] showed that the frictional resistance to sliding raises suddenly in response to an abrupt increase in effective normal stress and then continues to rise toward a new steady state value.

[17] In the present study, we aim to couple the temporal variations of friction coefficient and effective normal stress. To this goal, we need to use a constitutive law for fault friction that accounts for the normal stress variations. *Linker and Dieterich* [1992] performed quasi-static laboratory experiments with blocks of Westerly granite in a double-direct shear apparatus and interpreted the data by introducing the following generalization of the evolution law:

$$d\Psi = \left(\frac{\partial}{\partial u}\Psi\right)\Big|_{\sigma_n^{\text{eff}}} du - \left(\frac{\alpha_{\text{LD}}\Psi}{b\sigma_n^{\text{eff}}}\right) d\sigma_n^{\text{eff}} \tag{2}$$

where Ψ is the state variable, the dimensionless coupling parameter α_{LD} is estimated from experiments, b is the constitutive parameter (defined below) and the derivative in the first term on the right is computed taking the effective normal stress constant. This model incorporates the changes

in normal stress in the evolution of the state variable and these sudden changes in Ψ are inversely proportional to the sudden change in σ_n^{eff}. In (2) it has been assumed that for small changes in normal stress, the steady state coefficient of friction is independent of normal stress and that the steady state value of state variable (Ψ^{ss}) is consistent with the earlier models. According to *Linker and Dieterich* [1992] (hereinafter referred to as LD92) the constitutive relation for the ageing model becomes

$$\begin{aligned} \tau &= \left[\mu_* + a\,\ln\left(\frac{v}{v_*}\right) + b\,\ln\left(\frac{\Psi v_*}{L}\right)\right]\sigma_n^{\text{eff}} \\ \frac{\mathrm{d}}{\mathrm{d}t}\Psi &= 1 - \frac{\Psi v}{L} - \left(\frac{\alpha_{\text{LD}}\Psi}{b\sigma_n^{\text{eff}}}\right)\frac{\mathrm{d}}{\mathrm{d}t}\sigma_n^{\text{eff}} \end{aligned} \tag{3}$$

where a and b and L are the constitutive parameters, which we consider here being independent of the effective normal stress and temperature. In other words, we assume that these parameters are constant during the short durations of coseismic processes studied in this paper; μ_* and v_* are reference values for the friction coefficient and for the slip velocity v, respectively. Although equation (3) includes normal stress changes, we refer in the following of the paper to this law as the Dieterich-Ruina law (DR).

[18] In this study (results are shown in BC06) we also use the slip law [see *Beeler et al.*, 1994], which differs from (3) only for the state variable evolution law:

$$\begin{aligned} \tau &= \left[\mu_* + a\,\ln\left(\frac{v}{v_*}\right) + b\,\ln\left(\frac{\Psi v_*}{L}\right)\right]\sigma_n^{\text{eff}} \\ \frac{\mathrm{d}}{\mathrm{d}t}\Psi &= -\frac{\Psi v}{L}\ln\left(\frac{\Psi v}{L}\right) - \left(\frac{\alpha_{\text{LD}}\Psi}{b\sigma_n^{\text{eff}}}\right)\frac{\mathrm{d}}{\mathrm{d}t}\sigma_n^{\text{eff}} \end{aligned} \tag{4}$$

In the following, we refer to this relation as the Ruina-Dieterich (RD) law. The state variable Ψ included in (3) and (4) should be also considered as a macroscopic variable, similarly to shear stress and slip. According to *Dieterich* [1978] and *Linker and Dieterich* [1992] the state variable depends on the slip rate, that we consider here a macroscopic frictional slip velocity. Although the state variable has been originally interpreted to represent the state of the sliding surface, in this study we intend Ψ to be representative of the mechanical state of the whole slipping zone [see also *Sleep*, 1997].

[19] We emphasize here that the temporal variation of the effective normal stress, included both in (3) and (4), can be due to (1) an imposed load condition, as in LD92 and *Dieterich and Linker* [1992]; (2) a previous seismic event that modifies the state of the stress along the actual fault [see, e.g., *Perfettini et al.*, 1999, 2003; *Antonioli et al.*, 2006]; (3) a bimaterial fault in which the two halves of the fault plane have different elastic properties [*Andrews and Ben-Zion*, 1997; *Harris and Day*, 1997], or, finally, (4) a consequence of pore fluid pressure variation due thermal pressurization, which is controlled by different physical mechanisms. In the remainder of the paper we focus on the last phenomenon.

4. Thermal Pressurization Model

4.1. Frictional Heating

[20] We compute the temperature changes caused by frictional heating within a slipping zone whose thickness is $2w$. To this goal, we solve the 1-D Fourier's equation of heat conduction for a thermally isotropic medium, when the state changes [*Stefan*, 1891] are not considered:

$$\frac{\partial}{\partial t}T = \chi\frac{\partial^2}{\partial\zeta^2}T + \frac{1}{c}q \tag{5}$$

where ζ is the spatial coordinate normal to the fault (see Figure 1b), χ is the thermal diffusivity ($\chi = \kappa/\rho_{\text{bulk}}\mathcal{C}_{\text{bulk}_p}$, where κ is the thermal conductivity, ρ_{bulk} is the cubic mass density of the bulk composite and $\mathcal{C}_{\text{bulk}_p}$ is the specific heat of the bulk composite at constant pressure), $c \equiv \rho_{\text{bulk}}\mathcal{C}_{\text{bulk}_p}$ is the heat capacity for unit volume of the bulk composite and q is the heat generated for unit volume and for unit time ($[q] = \text{J}/(\text{m}^3\,\text{s}) = \text{W}/\text{m}^3$). *Fialko* [2004] solved the same equation for his 2-D calculation of heat flow caused by frictional sliding. The solution of equation (5) is given in Appendix A. We report here the solution for the temperature evolution on the fault plane ($\zeta = 0$):

$$\begin{aligned} T^{w^f}(\xi_1,\xi_3,t) = T_0^f + \frac{1}{2cw(\xi_1,\xi_3)}\int_0^{t-\varepsilon}\mathrm{d}t'\,\mathrm{erf}\left(\frac{w(\xi_1,\xi_3)}{2\sqrt{\chi(t-t')}}\right) \\ \cdot\,\tau(\xi_1,\xi_3,t')v(\xi_1,\xi_3,t') \end{aligned} \tag{6}$$

where T_0^f is the initial temperature distribution on the fault plane (i.e., $T_0^f \equiv T(\xi_1, 0, \xi_3, 0)$), erf( ) is the error function and ε is an arbitrarily small positive number. The temperature change on the fault plane is therefore given by $\Delta T = T^{w^f} - T_0^f$.

4.2. Thermal Pressurization of Pore Fluids

[21] In this section we compute the pore pressure evolution by solving constitutive equations for fluid flow. The formulation of this problem and the solution of the constitutive equations are described in detail in Appendix B. Pore pressure changes are associated with the temperature variations caused by frictional heating, the porosity evolution and the fluid transport through

$$\frac{\partial}{\partial t}p_{\text{fluid}} = \frac{\alpha_{\text{fluid}}}{\beta_{\text{fluid}}}\frac{\partial}{\partial t}T - \frac{1}{\beta_{\text{fluid}}\Phi}\frac{\partial}{\partial t}\Phi + \omega\frac{\partial^2}{\partial\zeta^2}p_{\text{fluid}} \tag{7}$$

where ω is the hydraulic diffusivity, which is

$$\omega \equiv \frac{k}{\eta_{\text{fluid}}\beta_{\text{fluid}}\Phi} \tag{8}$$

where k is the permeability of the medium, η_{fluid} is the dynamic fluid viscosity, Φ is the porosity, β_{fluid} is the coefficient of the compressibility of the fluid and α_{fluid} is the coefficient of thermal expansion of the fluid. As shown in Appendix B, for a constant porosity ($\Phi(\xi_1, \zeta, \xi_3, t) = \Phi_0(\xi_1, \zeta, \xi_3)$), the solution for pore pressure evolution in a generic fault point (ξ_1,ξ_3) and at a time t is obtained by solving equations (5) and (7); this gives

$$\begin{aligned} p_{\text{fluid}}^{w^f}(\xi_1,\xi_3,t) = p_{\text{fluid}_0}^f + \frac{\gamma}{2w(\xi_1,\xi_3)}\int_0^{t-\varepsilon}\mathrm{d}t' \\ \cdot\left\{-\frac{\chi}{\omega-\chi}\,\mathrm{erf}\left(\frac{w(\xi_1,\xi_3)}{2\sqrt{\chi(t-t')}}\right) + \frac{\omega}{\omega-\chi}\,\mathrm{erf}\left(\frac{w(\xi_1,\xi_3)}{2\sqrt{\omega(t-t')}}\right)\right\} \\ \cdot\,\tau(\xi_1,\xi_3,t')v(\xi_1,\xi_3,t') \end{aligned} \tag{9}$$

Table 1. Medium and Constitutive Parameters Adopted in This Study

Parameter	Value
Medium and Discretization Parameters	
$\lambda = G$	27 GPa
v_P	5196 m/s
v_S	3000 m/s
$\Delta x_1 = \Delta x_3$	25 m
Δx_2	100 m
Δt	0.83671×10^{-3} s
$\sigma_n - p^f_{\text{fluid}_0}$	30 MPa[a]
Slip-Weakening Model Parameters	
τ_0	20 MPa
μ_u	0.93333
μ_f	0.33333
S (at $t = 0$; reference)	0.8
d_0	0.1 m
Rate- and State-Dependent Models Parameters	
τ_0	$\tau^{ss}(v_{\text{init}})$
a	0.007
b	0.016
L	0.01 m
v_{init}	1×10^{-4} m/s
$\mu*$	0.56
Ψ_{nucl}	1×10^{-4} s
$\Psi_{\text{outside the nucleation}}$	$\Psi^{ss}(v_{\text{init}})$
α_{LD} (reference)	0.53
Thermal Pressurization Parameters	
T_0^f	100 °C [b]
k (reference)	5×10^{-17} m^2 [c]
η_{fluid}	1×10^{-4} Pa s [d]
c	3×10^6 J/(m^3 °C) [e]
χ	1×10^{-6} m^2/s [f]
Φ_0	0.025
α_{fluid}	1.5×10^{-3} °C^{-1}
β_{fluid}	1×10^{-9} Pa^{-1}
w (reference)	0.035 m [g]

[a]This value is representative of a difference between lithostatic and hydrostatic stress calculated at a depth of 2 km or greater if pore fluid pressures is above the hydrostatic level. See text for further details.

[b]This is a roughly estimate arising from the adiabatic temperature gradient and it has to be regarded as an average temperature on the fault plane.

[c]The permeability k used here may be considered as an average value in the slip and in the damage zones. Data from different fault zones show that k ranges between 10^{-16} m^2 and 10^{-22} m^2 [*Morrow et al.*, 1984; *Chester et al.*, 1993; *Ito et al.*, 1998; *Lockner et al.*, 2000; *Mizoguchi et al.*, 2000; *Wibberley and Shimamoto*, 2003].

[d]See *Andrews* [2002] and *Miller et al.* [2004]; *Miller* [2002] uses 1.9×10^{-4} Pa s.

[e]See *Andrews* [2002]. Using the values reported, the parameter $\gamma \equiv \alpha_{\text{fluid}}/(\beta_{\text{fluid}} c)$ is equal to 0.5 in all numerical experiments presented and discussed in this paper. The specific heat C_{bulk_p} is 1100 J/(kg °C).

[f]The same value used by *Cardwell et al.* [1978], *Fialko and Rubin* [1998], *Andrews* [2002] and *Fialko* [2004]; *McKenzie and Brune* [1972] use 7×10^{-7} m^2/s.

[g]This reference value is in agreement with those reported by *Chester* [1995] and *Fialko* [2004].

where $p^f_{\text{fluid}_0}$ is the initial fluid pressure distribution (i.e., $p^f_{\text{fluid}_0} \equiv p_{\text{fluid}}(\xi_1, 0, \xi_3, 0)$) and $\gamma \equiv \alpha_{\text{fluid}}/(\beta_{\text{fluid}} c)$. The effective normal stress can be expressed as

$$\sigma_n^{\text{eff}} = \sigma_n - p^{w^f}_{\text{fluid}} = \sigma_n - p^f_{\text{fluid}_0} - \Delta p^{w^f}_{\text{fluid}}, \tag{10}$$

where $\Delta p^{w^f}_{\text{fluid}}$ is the second term in the right member of equation (9). In this work both normal stress and pore fluid pressure are assumed to be negative for compression: this means that if $\hat{\mathbf{n}}$ is the unit vector normal to the fault surface (see Figure 1b), thus the normal traction acting on the fault is $\Sigma = -\sigma_n^{\text{eff}}\,\hat{\mathbf{n}}$. In the following, we consider as "dry" a fault in which there are no pore fluid pressure changes and therefore $\Delta p^{w^f}_{\text{fluid}} = 0$. In this case the effective normal stress is constant and equal to its initial value $\sigma_n - p^f_{\text{fluid}_0}$. On the contrary, when fluid flow is allowed ($\Delta p^{w^f}_{\text{fluid}} \neq 0$) outside the fault plane, we refer to a "wet" fault: in this case σ_n^{eff} is evolving through time.

[22] In sections 5 and 6 we present the results of several numerical experiments performed using different governing laws. In all these simulations the porosity is taken constant and we use the solutions described above in our numerical algorithm. The assumption of a constant porosity implies that additional physical effects might be neglected in our simulations; this is because temporal variations of dynamic porosity might counterbalance the effects of frictional heating and fluid flow, as stated in equation (7). We discuss this issue in BC06, where we have calculated the analytical solutions of the thermal pressurization problem accounting for porosity evolution (see Appendix A of BC06), and we discuss numerical experiments with time-dependent porosity.

4.3. Adopted Model Parameters

[23] In all numerical experiments presented and discussed in this and BC06 we assume a dimensional set of parameters typical of a real fault: medium, constitutive and model parameters are listed in Table 1. Faults governed by a SW law extend 4000 m both in the along strike and dip directions; the only exception is the model adopted for the simulations shown in Figure 2, for which the fault is 12,500 km both in the along strike and dip directions. Faults governed by RS laws extend 6250 m in the along strike and dip directions. The hypocenter is always located at the center of the fault.

[24] The initial value of the effective normal stress is 30 MPa. This value corresponds to a difference between lithostatic and hydrostatic stress calculated at a depth of nearly 2 km; however, if pore fluid pressure is greater than the hydrostatic value (it might also approach the lithostatic value [see, e.g., *Hubbert and Rubey*, 1959; *Berry*, 1973]), the adopted value can be representative of seismogenic depths greater than 2 km. The initial temperature is 100°C, and as all parameters, it has to be regarded as an average value on the fault plane. This value arises from the adiabatic temperature gradient. It is important to note that the initial temperature value (T_0^f) does not affect the obtained results, because temperature change and pressure change do not depend on the initial temperature value. In Table 1 we report several references regarding the adopted thermal pressurization parameters.

[25] Although a complete exploration of model and constitutive parameters is beyond the goals of the present study, in the following of this paper as well as in BC06 we discuss simulations performed by solving the thermal pressurization problem with different frictional parameters.

5. Temperature Changes Caused by Frictional Heating

[26] We have simulated the dynamic propagation of an earthquake rupture obeying the SW law accounting for the

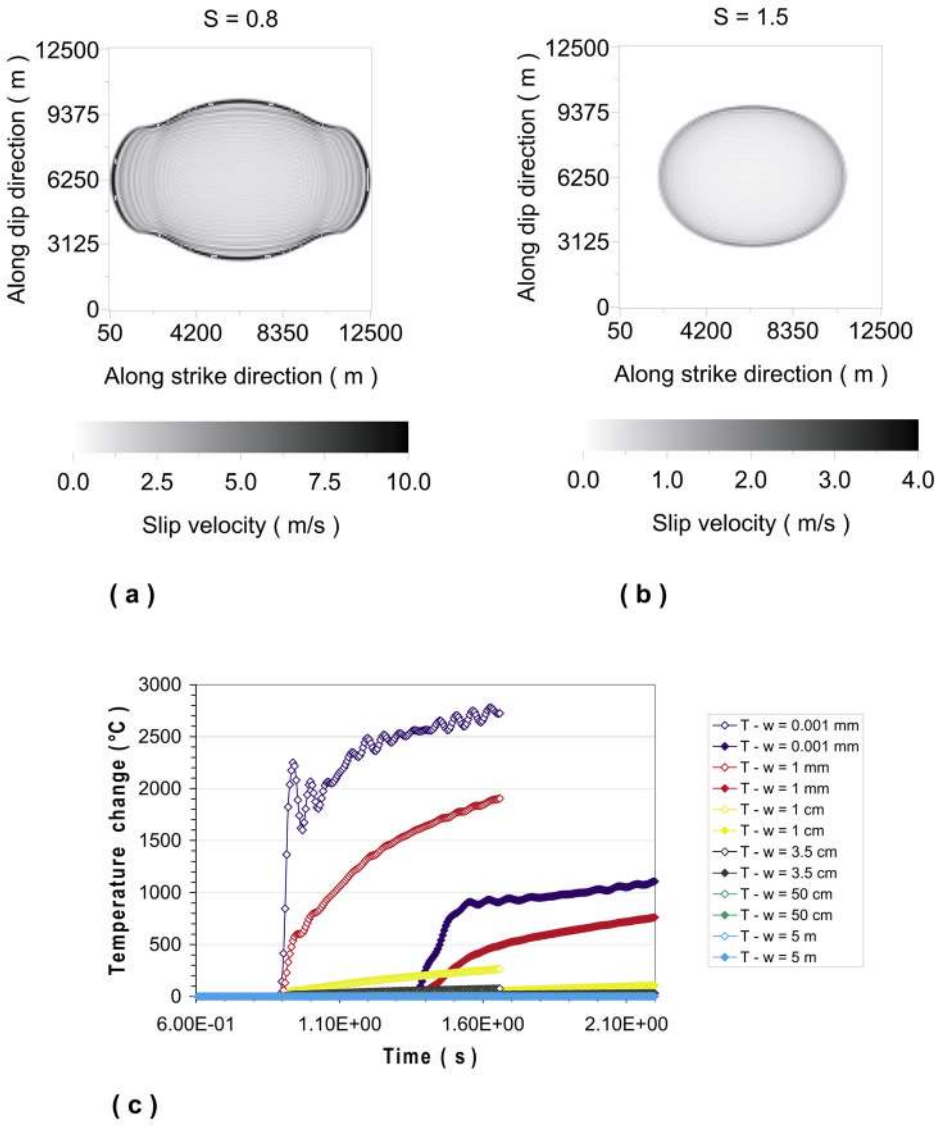

Figure 2. Snapshots of slip velocity on the fault plane at the last time step of the numerical simulations for (a) a low strength (S = 0.8) fault and (b) a high strength (S = 1.5) fault. A linear SW law has been adopted in these simulations. (c) Temperature time histories at a fault point (9000 m, 6200 m) for different values of slipping zone thickness $2w$. Open and solid symbols refer to low and high strength (S) configurations, respectively. Medium and constitutive parameters are listed in Table 1; the high strength fault has $\mu_u = 0.81667$ and $\mu_f = 0.56667$.

temperature changes due to frictional heating by using the solution shown in (6) and derived in Appendix A. Results of these calculations are illustrated in Figure 2, which shows the spatial pattern of slip velocity and the temperature change time histories in a target fault point for two values of the strength parameter

$$S \underset{\text{df}}{=} \frac{\tau_u - \tau_0}{\tau_0 - \tau_f} \tag{11}$$

[*Das and Aki*, 1977a, 1977b]. The time histories of temperature change are plotted for several values of the slip zone thickness ($2w$). For the same slip zone thickness, the temperature changes associated with the low value of the strength parameter (S = 0.8) are higher than those generated by the high strength (S = 1.5). This happens because slip velocity and the breakdown stress drop are higher for the low strength than for the high strength fault (the initial stress being the same for the two models). In the following, we compare these results with others obtained for different frictional configurations (i.e., different values of the strength parameter). As expected, the results presented in Figure 2 confirm that decreasing the slip zone thickness ($2w$) increases the temperature on the fault plane. These simulations point out that thermal pressurization affects the dynamic rupture propagation. We will further discuss this issue in section 6.

[27] We consider now a dry fault governed by the linear SW law (equation (1)); we plot in Figure 3 the temperature change history in a fault point, considering three different

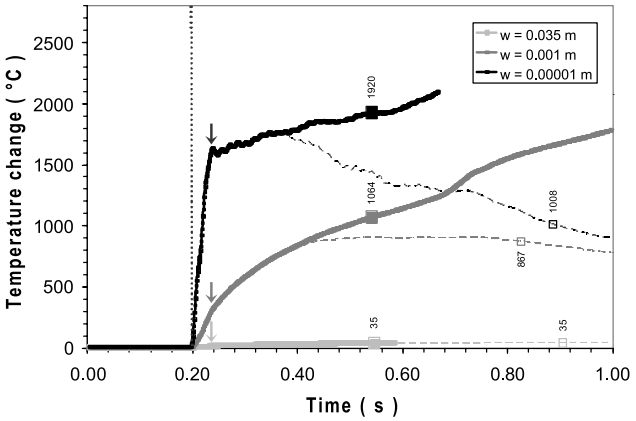

Figure 3. Temperature changes (i.e., measured with respect to the initial value T_0^f) as a function of time for dry faults (only caused by frictional heating) governed by the linear SW law and having different slipping zone thickness. For each w, solid curves refer to crack-like models (i.e., no healing of slip), while dashed curves refer to numerical experiments in which the slip duration is finite (with healing). In the latter case, we can identify the first time step at which the maximum total fault slip is reached, which is indicated by an open square in the dashed curves. In the solid curves, solid squares indicate the time step at which the fault has developed the same cumulative slip. Numbers indicate the temperature change values (°C) at those time steps. The vertical dotted line indicates the time step at which the traction on the fault reaches the upper yield value τ_u, while vertical arrows define, for each curve, the time step at which the fault slip velocity is at its maximum. Solutions are plotted in a fault point at a distance of 900 m from the hypocenter, at the depth of the hypocenter.

slipping zone thicknesses (w = 35 mm, 1 mm and 10 μm). For each w the solid curves refer to a crack-like models with no healing (i.e., infinite slip duration [see *Madariaga and Olsen*, 2000; *Bizzarri and Cocco*, 2005]), since the rupture does not arrest but propagates indefinitely. On the contrary, dashed curves refer to numerical experiments with heterogeneous faults, for which the slip duration is finite and therefore we have healing of slip. This heterogeneous configuration has been used to have healing of slip: in particular, rupture arrest is caused by a heterogeneous distribution of the initial shear stress characterized by a high value of strength parameter S in a region external to a circular area having a radius of 1300 m, centered at the hypocenter. We observe that before the rupture onset, temperature is equal to its initial value T_0^f, as expected from equation (6) for zero slip velocity; after the crack onset the temperature increases, depending on the value of the slipping zone thickness. Figure 3 shows that the initial sudden increase of temperature is the same with or without healing, because it is driven by the slip velocity evolution. After the initial change, temperature further increases before decreasing when slip starts healing. Moreover, temperature changes are relevant only for thin slipping zones: for a slipping zone thickness larger than 0.01 m the temperature changes are negligible. In the heterogeneous cases of Figure 3, we indicate the time step at which the maximum fault slip is reached and we report the associated temperature change value. For the homogeneous configuration (solid curves in Figure 3) we indicate the time step at which the fault has developed the same cumulative slip and the associated temperature change value. We note that in general the temperature changes are larger and faster for the crack-like solutions: for the same slip value, temperature change is larger than that inferred for the finite slip duration models (i.e., with healing of slip).

[28] We show in Figure 4 the spatial pattern of temperature changes (still with respect to the initial value T_0^f) on the fault plane computed for a crack model obeying to a SW friction law. In this set of simulations we also account for the thermal pressurization of pore fluids. In Figure 4a we plot the temperature evolution at a fixed time step as function of the spatial coordinate along the strike at the hypocentral depth: solid symbols refer to simulations with thermal pressurization (the effective normal stress σ_n^{eff} changes with time), while open symbols refer to dry configurations (normal stress is constant and equal to its initial value, $\sigma_n - p^f_{\text{fluid}_0} = 30$ MPa). We observe that thermal pressurization increases the effects of frictional heating: this is due to the effective normal stress reduction caused by pore pressure increase. We also display in Figure 4b the temperature changes on the fault plane for the simulation with 2 mm thickness (w = 1 mm) and thermal pressurization: this snapshot is taken at 0.38 s from the rupture nucleation. The estimates of temperature changes obtained in our 3-D model for dry configurations are in agreement with the values reported by *Fialko* [2004]. It is interesting to point out the particular shape of the temperature change pattern: the highest temperature rise does not coincide with the fault patch having the longest slip duration, because it is controlled by changes in fault slip velocity.

[29] In order to further discuss the effect of thermal pressurization, we show in Figure 5 the comparison between the temporal evolutions for dry and wet faults in the same target fault point for the same three values of slipping zone thickness used in Figure 3. We compare dry and wet faults (black and gray curves, respectively), as well as crack-like and healing-like cases (solid and dashed curves, respectively). The solutions for the wet case, which includes the effects of thermal pressurization with constant porosity, display a trend very similar to those inferred for dry conditions, also shown in Figure 3, for both finite or infinite slip durations (healing and crack-like). The temperature changes for wet faults begin earlier than those for dry faults, because thermal pressurization of fluids makes the fault more unstable, as we discuss in section 6. For this reason, the temperature change can be faster at the very early stage for wet faults than for dry ones. Although our simulations are representative of a set of parameters, they confirm the general conclusion that thermal pressurization with constant porosity reduces the temperature increase on the fault caused by frictional heating.

[30] A very interesting outcome arises from Figure 5: the effect of the thickness of the slipping zone is much more important than the contribution of thermal pressurization. For a thick fault zone (w = 35 mm, Figure 5a) the temperature changes (ΔT) are of the order of 30°C (30% of the initial temperature value) for both dry and wet faults independently of slip duration. If the thickness of the slipping zone is smaller (w = 1 mm, Figure 5b), the

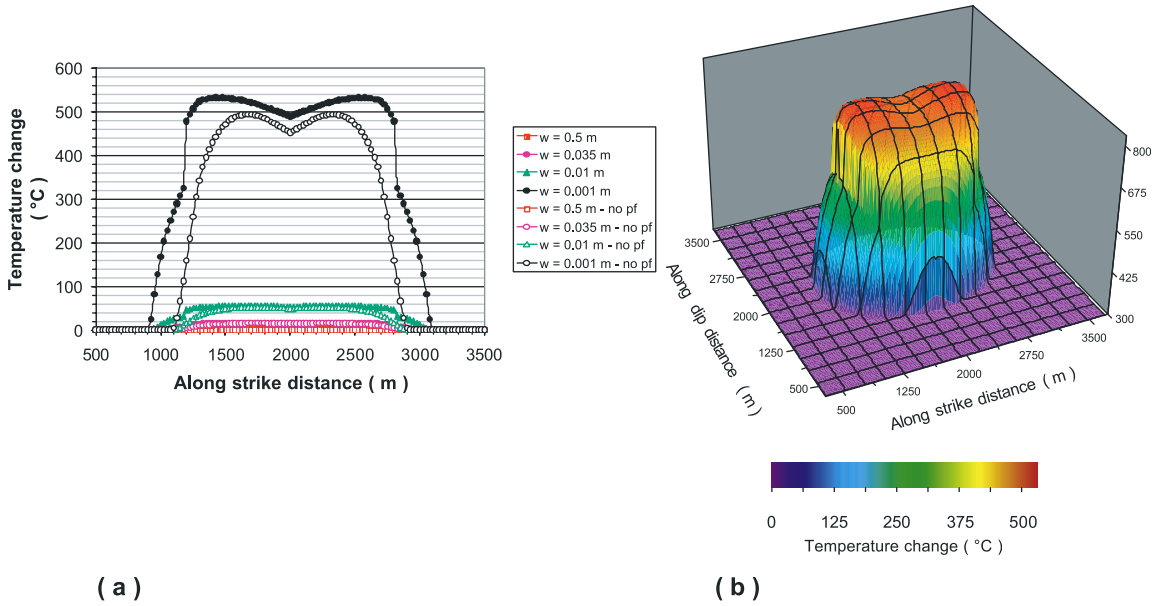

Figure 4. (a) Temperature changes for different slipping zone thicknesses due to frictional heating on a fault governed by the SW law. Solid symbols refer to rupture for which the temperature is coupled with fluid flow (i.e., numerical experiments with thermal pressurization), while open symbols refer to rupture without fluid effects. Each line is generated at the depth of the hypocenter. (b) Three-dimensional spatial distribution on the fault plane of the temperature changes for a particular case of Figure 4a (w = 1 mm, with thermal pressurization effects). Both Figures 4a and 4b are at the same time step (after 0.38 s after the nucleation).

temperature for a dry fault with finite slip duration increases nearly up to 1000°C; when accounting for thermal pressurization the temperature is still close to 850°C. In both cases the temperature changes are larger than eight times the initial temperature value. A further decrease in thickness of the slipping zone (w = 10 μm, Figure 5c) further rises the temperature nearly up to 2000°C and 1600°C for dry and wet faults, respectively. These temperatures might produce melting of fault gouge; *Di Toro and Pennacchioni* [2004] suggest that rock composite melts at temperatures between 1100°C and 1550°C. *Otsuki et al.* [2003] estimated melting temperature for the Nojima fault ranging between 750°C and 1280°C. Our calculations suggest that to have melting of the gouge we need an extremely thin slipping zone: according to the model parameters adopted in this study we need $w \leq 1$ mm. In these simulations we have used a value of hydraulic diffusivity equal to 0.02 m^2/s, and the maximum slip is slightly less than a meter. It is important to mention that in the melting regime the temperature and the pore pressure evolution derived in this paper are no longer valid since additional effects come into play, e.g., when gouge melts it liberates latent heat and another mass balance equation should be considered. However, taking into account such complications is beyond the scope of the current work.

[31] It is worth noting that for a constant porosity, the difference between the temperature changes computed accounting for thermal pressurization (wet faults) and those in adiabatic conditions without thermal pressurization [see *Kanamori and Heaton*, 2000; *Sibson*, 2003] depends on the thickness of the slipping zone and on the value of cumulative slip. This is evident from Figure 6a, which illustrates the temperature changes as a function of slipping zone half thickness (w) and compares the results of our numerical simulations with linear SW governing law and pore pressurization (solid curves) with the theoretically predicted temperature changes computed for a fault that adiabatically shears without thermal pressurization (dashed curves). In the latter case the temperature change is expected to increase linearly with the cumulative fault slip u and decrease inversely with $2w$ according to the relation: $\Delta T^{(\mathrm{adiab})} \cong \tau_f u/2cw$. Moreover, Figure 6a shows that (1) the temperature changes obtained using our solution are in agreement with the inverse dependence on $2w$; (2) the theoretically predicted $\Delta T^{(\mathrm{adiab})}$ are smaller than ΔT resulting from SW and thermal pressurization, and this difference depends on the cumulative slip value: the larger the slip the smaller the difference; (3) only for relatively small values of the slipping zone thickness ($w \leq 1$ mm, for the set of parameters used in these simulations) does thermal pressurization reduce the temperature changes. These results can be explained if we consider that for small slip values thermal pressurization with no porosity evolution generates larger stress drop and larger slip velocity yielding higher temperature changes than the adiabatic predictions. Moreover, these results can be also explained by noticing that while the adiabatic predictions with no pore pressurization contains the residual value of shear stress (τ_f), the temperature change inferred from the simulations with SW and thermal pressurization depends on stress amplitudes that vary with slip. Hence the simulations performed in this study contain much larger values of shear stress (traction at the beginning of the simulation is three times larger than τ_f) for significant part of the slip. This difference is more relevant for small

slip values (compared to the characteristic SW distance). Figure 6b reveals that neglecting porosity evolution, the temperature changes do not vary with the adopted values of hydraulic diffusivity. We discuss the implications of these results for melting of fault gouge materials in section 7.

6. Rupture Propagation With Thermal Pressurization

[32] In section 5 we presented the results of several numerical simulations performed using a SW constitutive law in which the traction evolution is prescribed within the cohesive zone. In this section we aim to discuss the effects of thermal pressurization of pore fluids caused by frictional heating using different constitutive laws, as the RS constitutive formulation. The assumed constitutive law controls the initial stages of dynamic fault weakening and slip acceleration; once slip velocity increases, temperature changes (as discussed in section 5) and produces an increase of pore pressure that modifies the effective normal stress. Figure 7 shows the pore pressure evolution for different fault zone thickness and hydraulic diffusivity values obtained by modeling thermal pressurization in fault models governed either by SW (Figures 7a and 7b) and DR (Figures 7c and 7d) constitutive laws. All these simulations have been performed with a constant porosity. The adopted parameters are listed in Table 1; we emphasize that we have chosen a characteristic length scale parameter L for RS that is one order of magnitude smaller than d_0 in SW: this agrees with the scaling between the equivalent SW distance d_0^{eq} and L proposed by *Cocco and Bizzarri* [2002] and *Bizzarri and Cocco* [2003]. Figure 7 illustrates that decreasing the slipping zone thickness as well as the hydraulic diffusivity value causes pore pressure increases with time, producing a temporal reduction of the effective normal stress. Our simulations reveal that the shape of the pore pressure temporal evolution depends on the adopted friction law. RS laws always produce a nearly constant pore pressure evolution after the end of the breakdown process (when the traction is at the kinetic stress level). Looking at the pressure increase, we can observe that for the same values of w and ω, SW produces a more abrupt increase at the rupture onset but a lower final level with respect to DR.

[33] In Figure 8 we compare the rupture evolution obeying the SW law with and without thermal pressurization effects. As in the previous numerical experiments, we assume that the porosity Φ does not change in time and its value equals the initial one. Figures 8a and 8b refer to a reference configuration in which fluid effects are ignored (dry case) and therefore the effective normal stress is constant over time. On the contrary, in Figures 8c and 8d

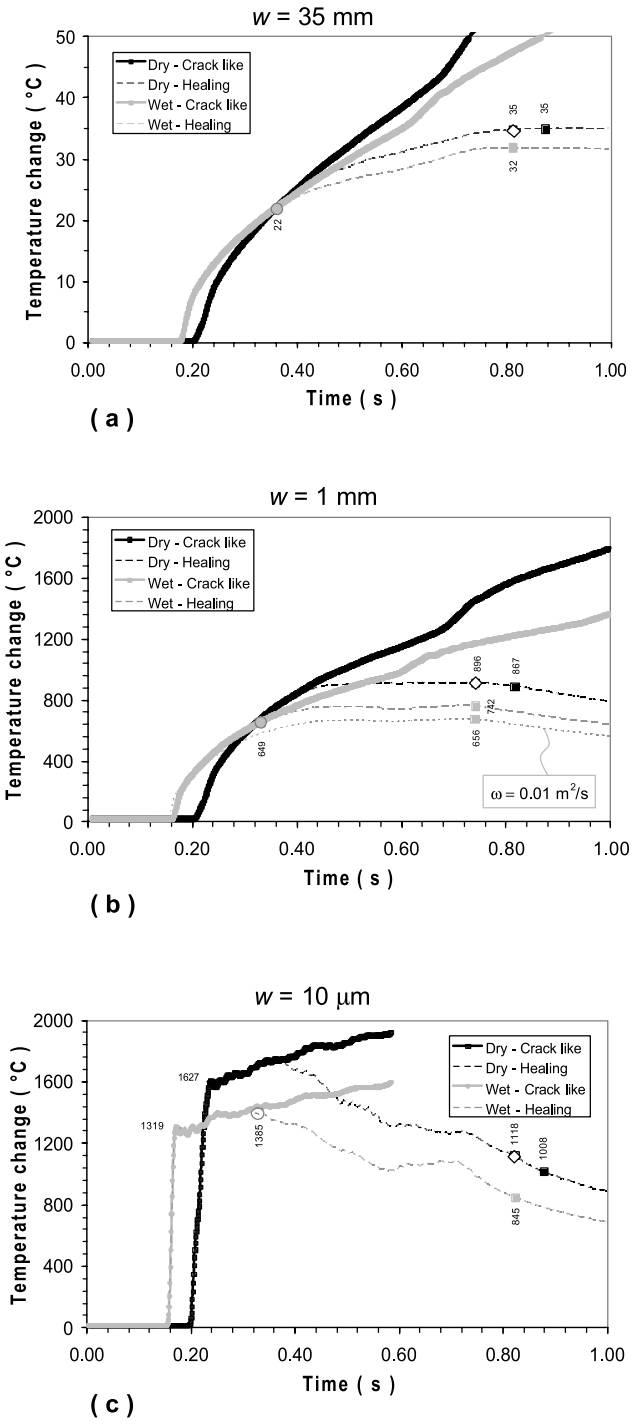

Figure 5. Temperature changes as a function of time for three different slipping zone half thicknesses: (a) $w = 35$ mm, (b) $w = 1$ mm, and (c) $w = 10$ μm, for a fault governed by the SW law. Black curves indicate dry faults, while gray ones refer to wet faults. Solid curves refer to crack-like solutions, and dashed curves refer to models with finite slip duration (healing of slip). For the latter cases, we have indicated with solid squares the time step at which the maximum fault slip is reached, and we report the temperature change values in degrees Celsius. In the dry case with healing of slip we have also indicated with open diamonds the corresponding time at which the slip saturates in the wet case (the fault slip velocity is zero). In the wet case with no healing (grey solid curves) we have indicated the temperature change when the fault has developed a value of the cumulative slip equal to the maximum slip in the wet case with healing (open gray circle). In Figure 5b we have also drawn a simulation for a dry fault with healing with hydraulic diffusivity equal to 0.01 m^2/s (dotted curve). Solutions are plotted in the same fault point of Figure 3.

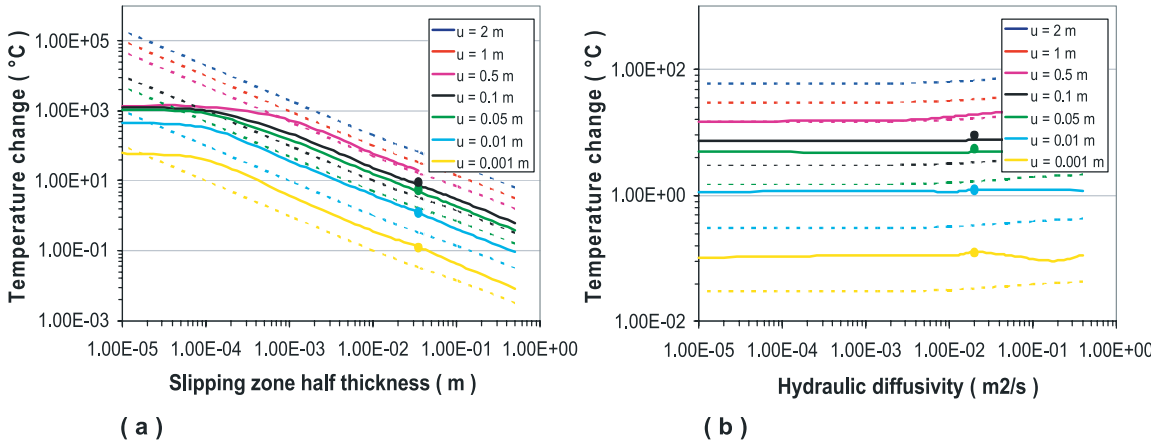

Figure 6. (a) Temperature changes as a function of the slipping zone thicknesses due to frictional heating on a fault governed by the SW law with thermal pressurization effects (solid curves). Each line represents a particular value of fault slip. Dashed lines refer to the adiabatic temperature changes neglecting thermal pressurization $\Delta T^{(\mathrm{adiab})} \cong \tau_f u/2cw$ [*Sibson*, 2003]; solid circles in each line indicate the values of temperature change in dry conditions, modeled in the numerical experiments for the reference value of slipping zone thickness (w = 0.035 m). (b) Temperature changes as a function of the hydraulic diffusivity (ω) and with the reference value of slip zone half thickness w. To change ω, we modify the permeability k. All solutions refer to the same fault point of Figure 3.

we plot the solutions for a fault in which thermal pressurization causes time variations of the effective normal stress (wet case). As we discuss in more detail in the following and in BC06, the wet fault is more unstable than the dry fault: at the same time step the wet fault has ruptured a broader region than the dry one. We emphasize that the inclusion of fluid pressurization causes more abrupt stress drop: we can observe from Figures 8b and 8d that the weakening phase is shorter for the wet fault and the weakening rate is higher than that inferred for the dry fault. This implies that the temperature change is faster. Figure 8 points out that thermal pressurization modifies the dynamic propagation of the earthquake rupture: for the same strength value (given by the value of the S parameter) a wet fault displays higher rupture velocities than the dry one and the rupture front acceleration to supershear speeds along the direction of the imposed prestress (Figure 8c).

[34] In Figure 9 we compare the solutions obtained adopting the Dieterich-Ruina law for dry and wet faults; in the former case the governing model is the original ageing law (because normal stress is constant), while the latter one is the modified DR law (defined in equation (3)), which includes the LD92 evolution law. Figure 9 shows that also in the framework of RS laws, thermal pressurization produces higher rupture velocity and slip rates, although the rupture front does not accelerate to a supershear speed as shown in Figure 8. In both cases the peak slip velocity does not corresponds to the equivalent kinetic frictional level, but it is reached before, especially in the dry case, confirming the findings of *Tinti et al.* [2004].

[35] The temporal evolution of dynamic traction and slip velocity illustrated in Figure 9 reveals that thermal pressurization with constant porosity produces a shorter duration of the breakdown process (of about 60%), similarly to what observed for a SW law. The evolution of the state variable when thermal pressurization affects the effective normal stress is very different. This is evident in Figure 10, where we plot the state variable time evolution for both the dry and wet cases; for the dry fault (black curves) the state variable starts from its initial configuration (assumed to be the steady state) and then smoothly decreases reaching a final state, that is still a steady state (in agreement with previous 2-D numerical simulations by *Bizzarri and Cocco* [2003] and with laboratory observations [see, e.g., *Wang and Scholz*, 1983]). Conversely, for the wet fault (gray curves) the fluid pressure changes cause an initial abrupt increase of the state variable during the breakdown time and then a fast decrease to the steady state. In BC06 we discuss how this different evolution of the state variable affects the dynamic traction evolution.

[36] In Figure 11 we show the results of several simulations performed by using either a SW law (Figures 11a, 11c, and 11e) or a DR friction law (Figures 11b, 11d, and 11e); solid squares and open circles identify dry and wet fault conditions, respectively. We plot in Figure 11 the friction coefficient ($\tau/\sigma_n^{\mathrm{eff}}$) as a function of time (Figures 11a and 11b), of the fault slip (Figures 11c and 11d) and, only for the wet cases, of the ratio between pore fluid pressure and nominal normal stress (i.e., Stribeck curve, Figures 11e and 11f). All parameters are those listed in Table 1, with the exception of slipping zone thickness that has been chosen equal to 2 mm (w = 1 mm). The solutions are calculated at the same target fault point used in Figures 3, 5, 6, 7, 8, 9, and 10. Figure 11 further confirms that the breakdown time for the wet simulations is shorter than that inferred for the dry ones and this effect is more pronounced for RS laws (see Figures 11a and 11b). Moreover, while for the SW solutions the drop of the friction coefficient does not change for the dry and wet faults, for the DR solutions it is larger for a wet fault. This is easily explained considering that only in the RS formulation the friction coefficient evolves in time and it can be also affected by normal stress variations through the state variable evolution (see equation (2)). On the

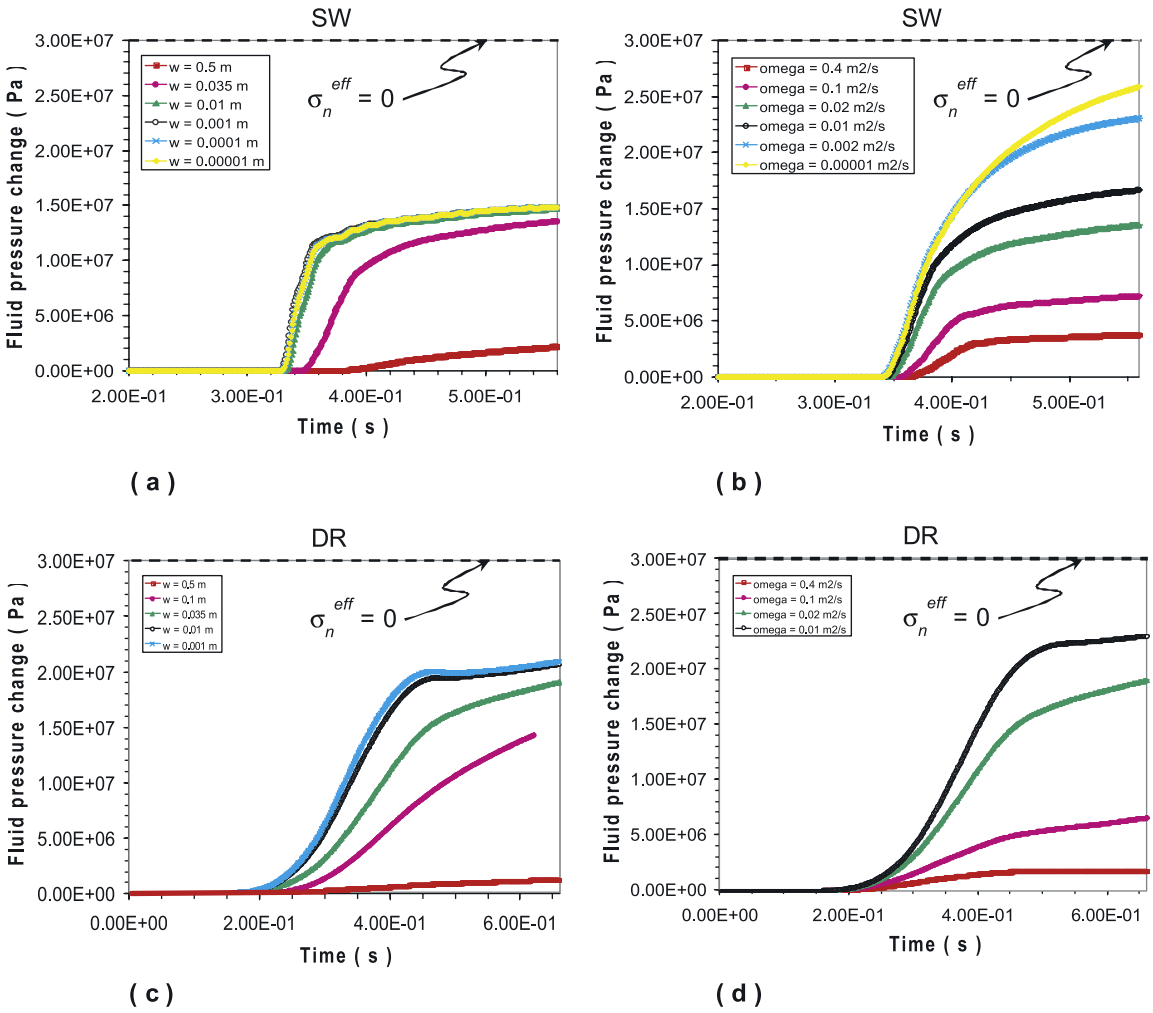

Figure 7. Pore fluid pressure change (with respect to the initial value of $\sigma_n - p^f_{\text{fluid}_0}$) as a function of time for a fault obeying (a and b) the SW law and (c and d) a DR law. In Figures 7a and 7c we have changed the slip zone thickness $2w$ (with respect to the reference configuration listed in Table 1). In Figures 7b and 7d we have changed the hydraulic diffusivity (ω) (through changes in permeability k). The horizontal dashed lines indicate the pore pressure value equal to the normal stress, which implies $\sigma_n^{\text{eff}} = 0$. Solutions are plotted in a fault point located at a distance from the hypocenter of 900 m (Figures 7a and 7b) and 1300 m (Figures 7c and 7d).

contrary, in the SW case the variation of the effective normal stress caused by thermal pressurization changes the value of the frictional stress level $\tau_f = \mu_f \sigma_n^{\text{eff}}$, but not the value of the coefficient of friction μ_f, which in this case has an assigned value. This is a fundamental difference between SW and RS friction laws. Furthermore, Figures 11c and 11d point out that while the characteristic slip-weakening distance is fixed a priori when the SW law is adopted (and in this case it does not change in dry and wet numerical experiments), it changes dramatically between dry and wet faults for the RS formulation. We have obtained an equivalent SW distance d_0^{eq} of about 10 cm in the dry case and about 50 cm in the wet one. This larger value does not follow the scaling law between d_0^{eq} and L proposed in dry conditions by *Bizzarri and Cocco* [2003] because in that work they did not account for the effects of thermal pressurization caused by frictional heating. We discuss this issue more in detail in BC06.

[37] In Figures 11e and 11f we have drawn the Stribeck curve [*Spikes*, 1997], which represents the friction coefficient μ as a function of the Sommerfeld number [*Sommerfeld*, 1950]. The Sommerfeld number is given by the ratio between the pore pressure and the normal stress, that is, $So \equiv p^{wf}_{\text{fluid}}/\sigma_n = (p^f_{\text{fluid}_0} + \Delta p^{wf}_{\text{fluid}})/\sigma_n$. (If normal stress σ_n is equal to the lithostatic (overburden) pressure, So is often called pore fluid pressure factor and it is indicated with the symbol λ.) We observe that $So < 1$ for both the constitutive formulations; this means that for the set of parameters used in this study, pore fluid pressure is always smaller than normal stress (then $\sigma_n^{\text{eff}} > 0$). In this case we are in the boundary lubrication regime and we do not enter in the hydrodynamic lubrication range [*Brodsky and Kanamori*, 2001]. Although these simulations have been performed for a set of model parameters, this plot allows us to point out that the two constitutive formulations yield a completely different evolution of the friction coefficient. In fact our calculations

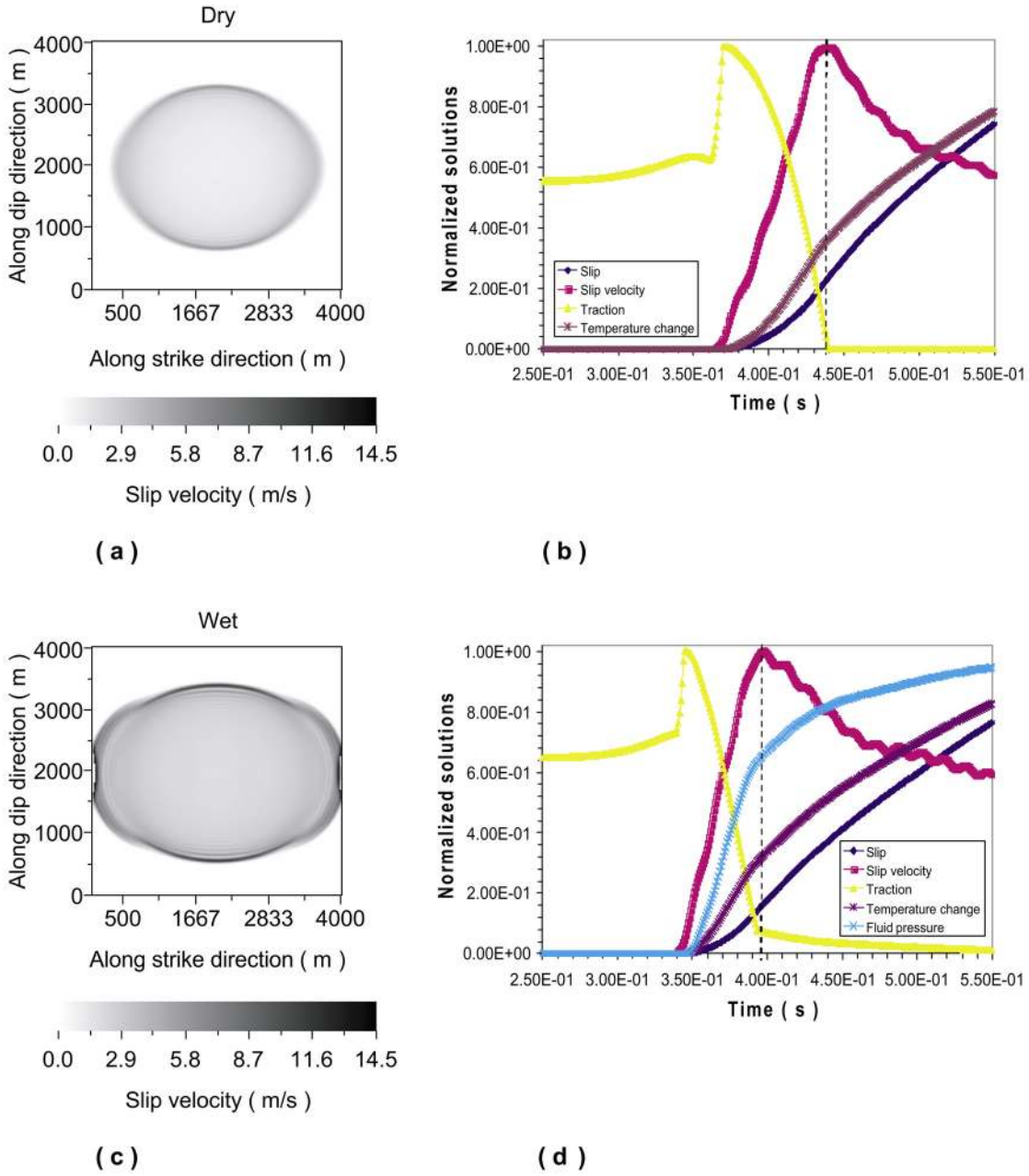

Figure 8. Slip velocity snapshots at the last time step of the numerical simulation for a rupture obeying to the SW constitutive equation (a) without and (b) with thermal pressurization effects. (c and d) Superposition of the solutions as a function of time in the two different configurations in the same fault point of Figure 3. All quantities are normalized with respect to their absolute maximum, with the exception of traction τ that is normalized as follows: $(\tau - \tau_{max})/(\tau_{max} - \tau_{min})$. Vertical dashed lines indicate the time step at which the maximum value of the slip velocity is reached.

show that while for the SW the friction coefficient always decreases after the initial increase due to the loading from other points on the fault (see Figure 11e), in the DR case the Stribeck curve displays a nearly linear increase of friction coefficient with the Sommerfeld number up to its peak value, which is followed by a fast drop. However, RS yields a larger pore pressure variation and therefore the values of the Sommerfeld number are greater than those obtained adopting the SW governing law. In other words, for the set of model parameters used in this study and for a constant porosity, the effective normal stress is smaller in the simulations performed using the RS formulation than those which use the SW law. In BC06 we discuss in detail how the variation of the fluid pressure affects the behavior of the dynamic traction evolution within the breakdown zone.

7. Discussion and Concluding Remarks

[38] In this paper we have analytically solved the 1-D thermal pressurization problem and applied it to model the

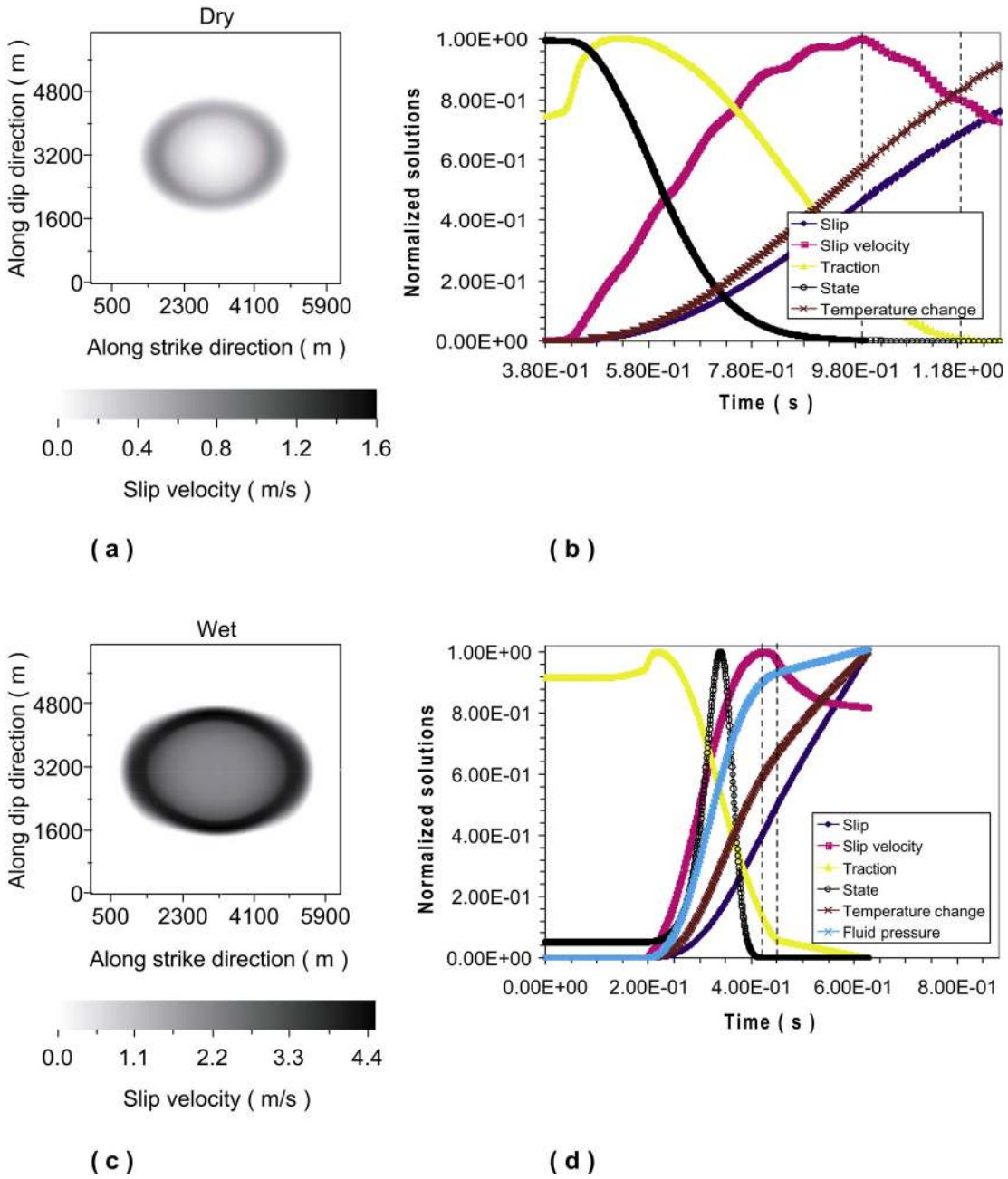

Figure 9. Same as Figure 8, but for dry and wet faults governed by DR friction law. Solutions are plotted in the same fault point of Figures 7c and 7d. Vertical dashed lines indicate the time step at which the maximum value of the slip velocity and of the kinetic frictional level are reached.

fully dynamic, spontaneous propagation of a truly 3-D earthquake rupture on a planar strike-slip fault. The frictional heating is represented by the temperature increase caused by coseismic slip episodes on the fault plane; this generates a fluid migration in the direction normal to the fault plane, which we model by coupling the thermal conduction equation and the Darcy's law for fluid flow. We consider only coseismic frictional heating (see equation (A2)), but in general the heat sources can be also modified to represent the heat generated during time-dependent compaction or ductile processes [*Beeler and Tullis*, 1997]. This in turn causes modifications of the effective normal stress affecting fault friction. We have extended to a 3-D fault framework the frictional heating model proposed by *Cardwell et al.* [1978] and recently applied to a nonspontaneous 2-D crack problem by *Fialko* [2004]. Our analytical solution of the thermal pressurization problem differ from that proposed by *Andrews* [2002] because we include a heat source appropriate for a fault of finite width and different constitutive relations: time-weakening or linear slip-weakening laws, as well as rate- and state-dependent friction laws with temporally varying effective normal stress.

[39] We have demonstrate that in a 3-D fault model and adopting different constitutive laws thermal pressurization

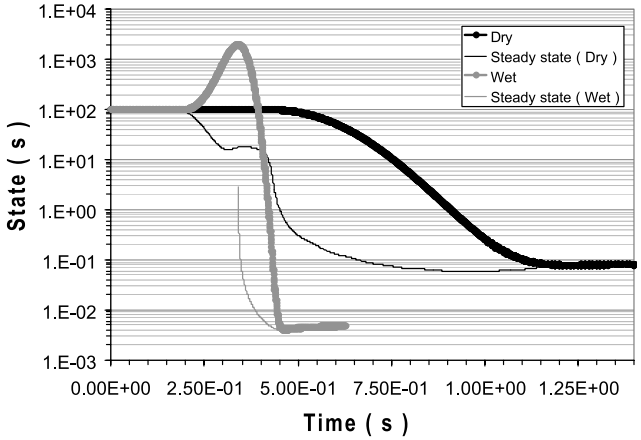

Figure 10. State variable evolution for the configurations showed in Figure 9. Black curves refer to dry faults, while gray ones to wet faults. Solid curves are the results of the numerical experiments, and thin lines represent the steady state value (Ψ^{ss}) of the state variable.

can play a very important role in the dynamic rupture propagation. Frictional heating and consequent pore fluid pressure changes are able to alter the traction evolution during the breakdown process, by modifying (with respect to a dry fault) the shape of the crack tip and the extension of the fractured zone at the same time step, complicating the time evolution of the friction coefficient. We further investigate some of these issues in BC06. We point out here that pore fluid pressure changes driven by coseismic frictional heating increases the breakdown stress drop and reduces fault friction.

[40] The numerical experiments discussed in this study have been performed with the governing parameters listed in Table 1. Although it is beyond the goals of this paper the comparing the behavior of wet faults adopting SW and RS constitutive laws, we present here temperature and pore fluid pressure changes calculated for a thermal pressurization model with constant porosity using both a linear SW and RS friction laws, but different values of constitutive parameters. The results are presented: Figures 12a and 12c show the temperature and pore fluid pressure changes computed adopting a linear SW law with three different values of the strength parameter S for dry and wet configurations; Figures 12b and 12d depict the same quantities calculated using the DR friction law with different combinations of the a and b parameters. These calculations confirm that thermal pressurization on a fault governed by a DR friction law causes a more pronounced pore fluid pressure change with respect to one obeying the SW law, but frictional heating does not strongly depend on the adopted values of the a and b constitutive parameters. On the other hand, the temperature changes calculated for a dry fault governed by a linear SW law depends on the adopted strength parameter S: the larger the breakdown stress drop and slip velocity the higher the temperature increase. In this latter case, the effect of thermal pressurization produces similar temperature and friction changes. In all these simulations the fault is more unstable when the strength parameter or the difference $(b - a)$ is larger.

[41] Our simulations suggest that the effect of the adopted fault zone thickness is more important than thermal pressurization in controlling the temperature changes caused by dynamic sliding episodes. *Fialko* [2004] has shown that the effective thickness of the slipping zone controls the temperature changes and the location where this perturbation occurs on the fault plane. This author concluded that thermal effects are expected to be significant for fault with highly localized slipping zones: if the slipping zone thickness is of the order of 1 mm, the temperature changes can be even larger than 1000°C, thus causing melting of fault gouge. Thermal pressurization has been proposed in the literature as a viable mechanism to reduce the temperature increase and to prevent melting [*Sibson*, 2003; *Fialko*, 2004]. The results of our study confirm that thermal pressurization reduces the temperature rise. However, if the thickness of the slipping zone is extremely thin, the increase of temperature is still large when thermal pressurization is taken into account: for half meter of slip in 1 mm of slipping zone thickness, the temperature change is still of the order of 800°C. In these simulations the thickness of the thermal boundary layer is of the order of 6 mm (corresponding to a thermal diffusivity of 10^{-6} m^2/s and 10 s of slip duration). It is important to remark here that this might be due to the fact that we consider constant permeability and porosity values, which do not change within the damage zone. In BC06 we show the results of several simulations performed considering the temporal evolution of porosity, as described in Appendix A of BC06.

[42] One important implication emerging from our numerical simulations is that thermal pressurization with constant porosity can reduce the fault resistance resulting in a substantial dynamic fault weakening. Nevertheless, for fault zones characterized by a relatively thin slipping zone the temperature changes computed with a thermal pressurization model with constant porosity are of the order of 800°C and can still be sufficiently large to generate melting of gouge materials. Two distinct thermally activated mechanisms can produce a drop in the friction coefficient and melting: thermal pressurization and flash heating of contact asperities of fault. We emphasize that these two mechanisms are substantially different: in fact, melting caused by thermal pressurization should be considered as a macroscopic phenomenon involving the whole effective slipping zone thickness. On the contrary, flash heating [*Rice*, 1999, 2006] is due to the highly localized heating created by a fast slip episode in the region near the moving asperity contacts on the slipping surface; in other words, it is generated on a relatively small contact area that sustains high shear strength. Under these conditions, the sudden and local increase of temperature causes a diminution of the contact's shear strength and a friction drop with slip rate. This might explain the experimental results of *Di Toro et al.* [2004]. Another difference between thermal pressurization and flash heating is that while the former strongly depends on the effective normal stress changes, the latter does not strongly change with normal stress. This because in the latter case the affected zone is very small and extremely thin, thus the capacity to support normal stress and the net area of contact might not be affected [*Rice and Cocco*, 2006]. It is important to remark that if melting occurs, the Terzaghi effective stress law is not anymore valid to represent the frictional properties of the fault zone.

[43] The numerical experiments presented in this study show that the hydraulic diffusivity strongly affects the

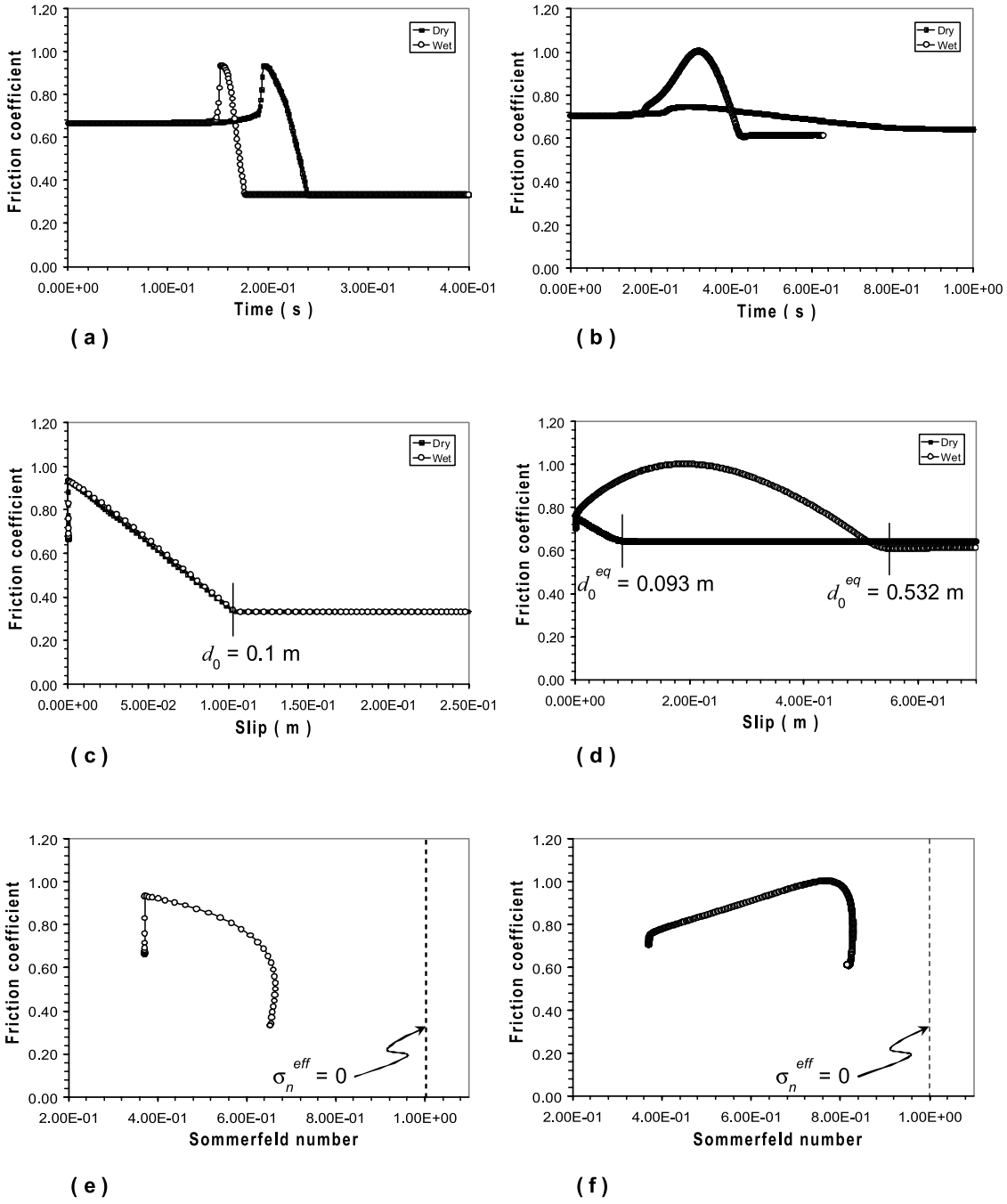

Figure 11. Friction coefficient ($\tau/\sigma_n^{\text{eff}}$) as a function of (a and b) time and (c and d) fault slip for dry and wet faults (open and solid symbols, respectively). (e and f) Stribeck curve for wet faults, which is the friction coefficient as a function of the Sommerfeld number (i.e., the ratio between pore fluid pressure and nominal normal stress). Plots refer to dry and wet faults governed by SW law (Figures 11a, 11c, and 11e) and by DR law (Figures 11b, 11d, and 11f). Dashed vertical lines in Figures 11e and 11f indicate the lithostatic pore pressure value. In Figures 11c and 11d the value of the characteristic SW distance is indicated by the vertical segment. Solutions are in the same fault point of Figure 3 for SW simulations and of Figures 7c and 7d for DR ones. Parameters are the same of those listed in Table 1, with the exception of slipping zone half thickness that now is w = 1 mm.

traction evolution and pore pressure changes, in agreement with the results shown by *Andrews* [2002]. This is expected because the pore pressure increase depends on the fluid flow outside the fault plane. Our results show that if the hydraulic diffusivity value is similar or slightly larger than thermal diffusivity, the pore pressure rise causes a relevant reduction of the effective normal stress (see the simulations shown in Figure 7). This would produce large rupture velocities, which might become supershear, and a nearly complete stress drop, as we discuss in detail in BC06. The pore fluid

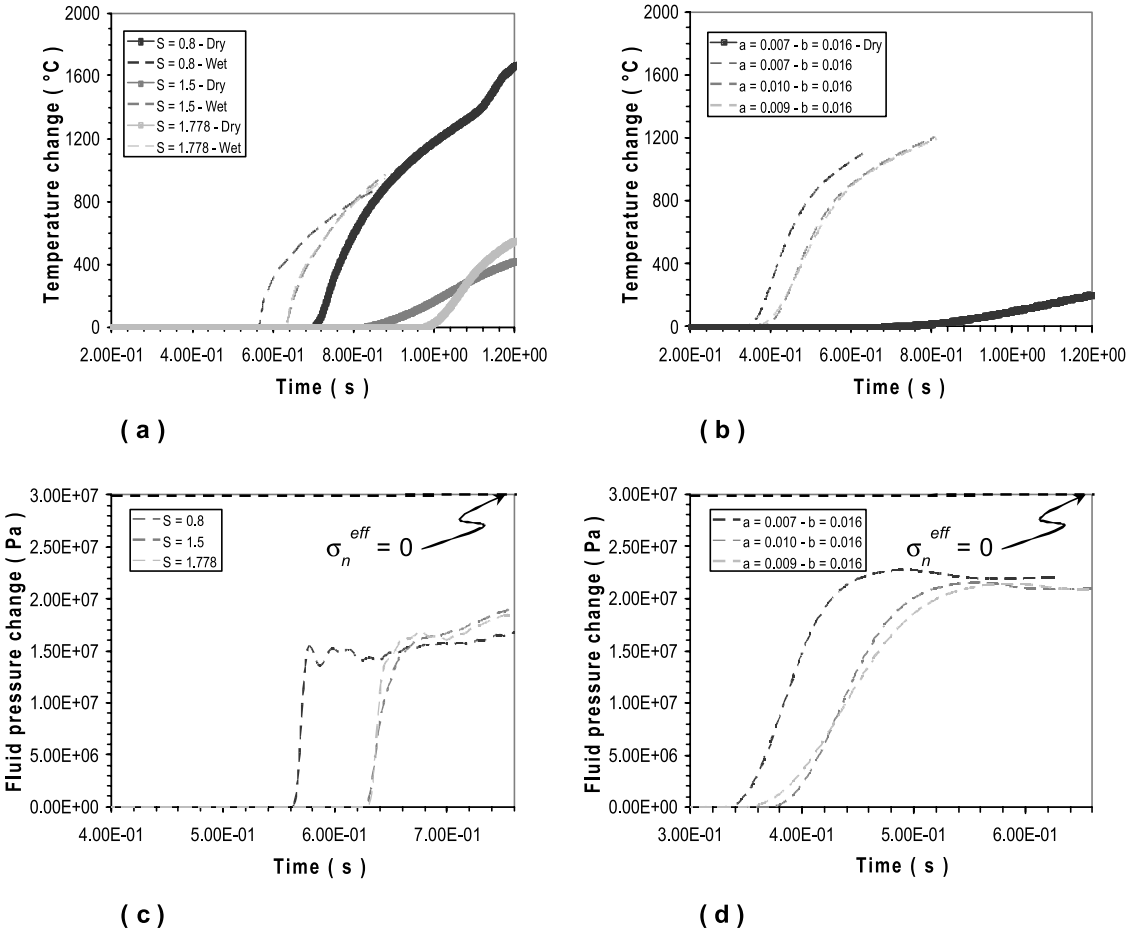

Figure 12. Temperature and pore fluid pressure changes computed adopting (a and c) a linear SW law and (b and d) the DR law. Solid curves refer to dry faults (i.e., no thermal pressurization), while dashed ones refer to wet ones (with thermal pressurization and constant porosity). These solutions are calculated in a fault point located at a distance of 1875 m from the hypocenter and for a slipping zone half thickness $w = 0.001$ m. The SW simulations have been performed for three values of the strength parameter S: those with $S = 0.8$ represent the reference case, whose constitutive parameters are listed in Table 1. The other two constitutive configurations have $S = 1.5$, corresponding to $\mu_u = 0.81667$ and $\mu_f = 0.56667$, and $S = 1.778$, corresponding to $\mu_u = 0.93333$ and $\mu_f = 0.51667$. The values of a and b parameters used in the simulations with the DR law are indicated in the legend of each plot. All the other parameters are those listed in Table 1.

pressure changes as well as their effects on the friction evolution strongly depend on the assumed constitutive law. In the framework of rate- and state-dependent friction laws, the state variable evolution is strongly affected by thermal pressurization, showing a preliminary increase followed by a sudden drop to the new steady state value. Thermal pressurization with constant porosity produces a faster and larger drop of the state variable affecting the evolution of the friction coefficient. We emphasize here that the use of a rate- and state-dependent constitutive law has the advantage of including the effects of effective normal stress variations in the temporal evolution of the friction coefficient, which is not allowed if a slip-weakening law is adopted. However, further investigations are needed to understand the best approach to include temporal changes of effective normal stress in the state variable evolution. We further investigate the effects of thermal pressurization on the main physical parameters controlling the traction evolution and the dynamic rupture propagation (breakdown stress drop, critical slip-weakening distance and fracture energy) in BC06. We conclude by pointing out that the analytical solution of the frictional heating problem implies the assumption that all the work spent in allowing the crack advance and fault sliding is heat. This raises a further question on the meaning of fracture when thermal pressurization controls the dynamic rupture propagation. We leave this issue for a more detailed discussion in BC06 and for future research.

Appendix A: Solution of the Thermal Conduction Problem

[44] In this appendix we derive the solution of the 1-D thermal conduction problem defined by equation (5). We denote with w the fault zone half width or, analogously, the

slip zone half thickness where the faulting process takes place (see Figure 1). The quantity $2w$ can also be interpreted as the slipping zone thickness and can be associated to the quantity $2D$ of *Andrews* [2002]. We also indicate with ξ_1 and ξ_3 the spatial coordinates on the fault plane and with ζ (namely, ξ_2) the coordinate normal to the fault.

[45] For an elementary heat source (i.e., point source in space and impulsive in time) of intensity $h(q^{el}(\zeta, t) \equiv h\delta(\zeta)\delta(t)$, where $[h] = J/m^2$ and $[q^{el}(\zeta, t)] = J/(m^3\ s) = W/m^3 = Pa/s$) the solution of equation (5) is [see *Carslaw and Jaeger*, 1959]

$$T^{el}(\zeta, t) = \frac{h}{2c\sqrt{\pi\chi t}} e^{-\frac{\zeta^2}{4\chi t}} \tag{A1}$$

The heat source (or the rate of frictional heat generation within the slipping zone) in a generic point of a fault (ξ_1, ξ_3) is expressed as the product of the shear stress τ and the shear strain rate. Accordingly to *Cardwell et al.* [1978] and *Fialko* [2004], we assume that the shear strain rate is constant within $2w$. *Mair and Marone* [2000] have shown with laboratory experiments that this hypothesis might be adequate. Therefore the shear strain rate becomes the ratio of the total slip velocity v over the thickness of the slipping zone $2w$. More complicated models in which the slip velocity profile may be nonlinear across the slipping zone can be considered, but they should be corroborated by new experimental results on the behavior of the slip zone and gouge evolution. Therefore the actual heat source q ($[q] = [q^{el}(\zeta, t)]$) is

$$q(\xi_1, \zeta, \xi_3, t) = \begin{cases} \dfrac{\tau(\xi_1, \xi_3, t)v(\xi_1, \xi_3, t)}{2w(\xi_1, \xi_3)}, & t > 0, |\zeta| \le w(\xi_1, \xi_3) \\ 0, & |\zeta| > w(\xi_1, \xi_3) \end{cases} \tag{A2}$$

In this relation it is implicitly assumed that all the work spent to allow the fault sliding is converted into heat [*Cardwell et al.*, 1978; *Scholz*, 2002; *Fialko*, 2004; *Di Toro et al.*, 2005]. This assumption maximizes the effect of the heat flux during the dynamic instability. Because we do not know how total energy is partitioned between frictional heating and surface energy [see also *Tinti et al.*, 2005], we cannot consider in our study alternative heat source models.

[46] The integral of $q(\xi_1, \zeta, \xi_3, t)$ over the normal coordinate ζ gives the heat flux, i.e., the heat produced per unit area on the fault and per unit time. In (A2) we explicitly state that the slipping zone may depend on the local coordinates and therefore it can change spatially; in our numerical experiments, however, we assume for simplicity that w is constant in space.

[47] The solution of equation (5) for this heat source is therefore determined by the Green's kernel corresponding to (A1). This leads to [e.g., *Morse and Feshbach*, 1953; *Cardwell et al.*, 1978; *Fialko*, 2004]

$$T^w(\xi_1, \zeta, \xi_3, t) = T(\xi_1, \zeta, \xi_3, 0) + \int_0^t dt' \int_{-\infty}^{+\infty} d\zeta' \cdot \left\{ \frac{1}{2c\sqrt{\pi\chi}} \frac{1}{\sqrt{t-t'}} e^{-\frac{(\zeta-\zeta')^2}{4\chi(t-t')}} \right\} q(\xi_1, \xi_3, \zeta', t') \tag{A3}$$

Assuming that quantities c and χ are homogeneous over the normal local coordinate ζ, putting (A2) into (A3) we can write

$$T^w(\xi_1, \zeta, \xi_3, t) = T_0 + \frac{1}{4cw(\xi_1, \xi_3)} \int_0^{t-\varepsilon} dt' \cdot \left\{ \operatorname{erf}\left(\frac{\zeta + w(\xi_1, \xi_3)}{2\sqrt{\chi(t-t')}} \right) - \operatorname{erf}\left(\frac{\zeta - w(\xi_1, \xi_3)}{2\sqrt{\chi(t-t')}} \right) \right\} \cdot \tau(\xi_1, \xi_3, t')v(\xi_1, \xi_3, t') \tag{A4}$$

where $T_0 \equiv T(\xi_1, \zeta, \xi_3, 0)$ is the initial temperature distribution (i.e., the host rock temperature prior to faulting), erf( ) is the error function

$$\left(\operatorname{erf}(z) \underset{\text{df}}{=} \frac{2}{\sqrt{\pi}} \int_0^z dx e^{-x^2} \right)$$

and ε is an arbitrarily small positive real number. Simple algebra shows in fact that in the limit of $t \to t'$ the Green function in (A3) is null and therefore the contribution at $t = t'$ in the temporal convolution is null. This has important consequences because it states that in calculating the temperature change $T^w - T_0$, we can stop the temporal integration at an instant immediately before the actual time t. In other words, the contribution at time t in the temperature change depends only on the previous traction and slip velocity time histories.

[48] Equation (A4) is a generalization to a 3-D case of the solution proposed by *Fialko* [2004] for a 2-D crack. On the fault surface, i.e., for $\zeta = 0$, equation (A4) becomes

$$T^{wf}(\xi_1, \xi_3, t) = T_0^f + \frac{1}{2cw(\xi_1, \xi_3)} \int_0^{t-\varepsilon} dt' \operatorname{erf}\left(\frac{w(\xi_1, \xi_3)}{2\sqrt{\chi(t-t')}} \right) \cdot \tau(\xi_1, \xi_3, t')v(\xi_1, \xi_3, t') \tag{A5}$$

where T_0^f is the initial temperature distribution on the fault plane (i.e., $T_0^f \equiv T(\xi_1, 0, \xi_3, 0)$).

[49] It is interesting to note that in the limit of zero thickness slipping zone, taking into account the properties of the error function, we have

$$T^{0f}(\xi_1, \xi_3, t) = T_0^f + \frac{1}{2c\sqrt{\pi\chi}} \int_0^{t-\varepsilon} dt' \frac{\tau(\xi_1, \xi_3, t')v(\xi_1, \xi_3, t')}{\sqrt{t-t'}} \tag{A6}$$

which is analogue to the limit for $D \to 0$ of the solution obtained by *Andrews* [2002].

[50] The analytical relations presented above have been obtained by solving the 1-D heat flux problem considering only one spatial coordinate (i.e., the normal to the fault). This implicitly means that we do not account for the possible contributions to the temperature changes coming from the neighboring points. It is clear from equations (A4) and (A5) that the temperature value at time t in a specified fault point does not explicitly depends on the values of total traction and slip velocity on the whole fault plane, but only

on their values in the local position (ξ_1, ξ_3). Because we are solving a 3-D elastodynamic problem, we have verified this assumption.

[51] Let us consider now the 3-D thermal conduction problem

$$\frac{\partial}{\partial t}T = \chi\left(\frac{\partial^2}{\partial\xi_1^2}+\frac{\partial^2}{\partial\zeta^2}+\frac{\partial^2}{\partial\xi_3^2}\right)T+\frac{1}{c}q \tag{A7}$$

having the elementary solution

$$T^{el}(\xi_1,\zeta,\xi_3,t) = \frac{h}{c\sqrt{(4\pi\chi t)^3}}\mathrm{e}^{-\frac{\xi_1+\zeta^2+\xi_3}{4\chi t}} \tag{A8}$$

where the intensity h has now dimension of Joule ($[h]$ = J). Assuming the actual heat source q as in equation (A2), proceeding as in the derivation of equation (A4), we can write

$$\begin{aligned} T^{w}(\xi_1,\zeta,\xi_3,t) = T_0 &+ \frac{1}{4cw(\xi_1,\xi_3)}\int_0^{t-\varepsilon}\mathrm{d}t'\int_{-\infty}^{+\infty}\mathrm{d}\xi_1' \\ &\cdot\frac{\mathrm{e}^{-\frac{(\xi_1-\xi_1')^2}{4\chi(t-t')}}}{\sqrt{\pi}\sqrt{4\chi(t-t')}}\int_{-\infty}^{+\infty}\mathrm{d}\xi_3'\frac{\mathrm{e}^{-\frac{(\xi_3-\xi_3')^2}{4\chi(t-t')}}}{\sqrt{\pi}\sqrt{4\chi(t-t')}} \\ &\cdot\left\{\mathrm{erf}\left(\frac{\zeta+w(\xi_1,\xi_3)}{2\sqrt{\chi(t-t')}}\right)-\mathrm{erf}\left(\frac{\zeta-w(\xi_1,\xi_3)}{2\sqrt{\chi(t-t')}}\right)\right\} \\ &\cdot\tau(\xi_1',\xi_3',t')v(\xi_1',\xi_3',t') \end{aligned} \tag{A9}$$

where $T_0 \equiv T(\xi_1, \zeta, \xi_3, 0)$ is the initial temperature as in equation (A4). However, considering the short time window (the coseismic timescale) of the dynamic rupture process and the value of thermal diffusivity χ, we easily obtain

$$\begin{aligned} &\int_{-\infty}^{+\infty}\mathrm{d}\xi_1'\frac{\mathrm{e}^{-\frac{(\xi_1-\xi_1')^2}{4\chi(t-t')}}}{\sqrt{\pi}\sqrt{4\chi(t-t')}}\tau\left(\xi_1',\xi_3',t'\right)v\left(\xi_1',\xi_3',t'\right) \\ &\quad=\tau\left(\xi_1,\xi_3',t'\right)v\left(\xi_1,\xi_3',t'\right) \end{aligned} \tag{A10}$$

and an analogous expression for the integral involving the second on-fault coordinate (ξ_3).

[52] Therefore, taking into account these results, from (A9) we obtain equation (A4), and in the limit of $\zeta = 0$ we obtain equation (A5). In other words we have demonstrated that in the coseismic temporal scale, the 1-D (normal to fault plane) approximation of the thermal conduction problem is acceptable and that the temperature in a fault point mainly depends on the fault slip velocity and traction time histories in that point.

Appendix B: Solution of the Simplified Thermal Pressurization Problem

[53] The flow of fluids in the Earth crust occurs through a matrix of interconnected passages, represented either by small fractures in rocks and by voids of naturally porous rocks. According to *Turcotte and Schubert* [2002] we define porous media materials where the scale of the flow system is large with respect to the scale of the passages. The fraction of the material's volume made up of pore is known as porosity ($\Phi = V_{\mathrm{voids}}/V_{\mathrm{tot}}$). The resistance of a porous media to fluid flow depends on the permeability k that represents the tortuosity of the fluid pathways through the solid matrix (the dry skeleton): the more permeable the medium is, the larger k is. It can be determined by laboratory experiments or by in situ observations [*Lockner et al.*, 2000; *Wibberley and Shimamoto*, 2003].

[54] Fluids can flow through a porous material under the influence of the applied pressure gradient. If we assume that (1) the scale of the porosity is small compared with the other characteristic dimensions of the flow and (2) no advective terms are considered so that the flow in the individual channels is laminar, the fluid flow in a porous medium can be described by an empirical relationship known as Darcy's law [*Darcy*, 1856], that states that the flow through the porous material is linearly proportional to the difference between the pressure gradient and the hydrostatic pressure and inversely proportional to the viscosity of the fluid. Because of the small characteristic diffusion distances compared to the along strike variations in properties and forcing, i.e., as a consequence of the 1-D thermal conduction equations, we can assume that fluids flow in the direction perpendicular to the fault. Consequently, we have considered the 1-D version of the Darcy's law:

$$q_\zeta = -\frac{k}{\eta_{\mathrm{fluid}}}\frac{\partial}{\partial\zeta}p_{\mathrm{fluid}} \tag{B1}$$

where q_ζ is the volumetric flow rate per unit area, $(\partial/\partial\zeta)p_{\mathrm{fluid}}$ is the fluid pressure gradient along the direction perpendicular to the fault and η_{fluid} is the dynamic viscosity of the fluid. (In the case of a dipping fault equation (B1) contains also the projection on ζ of the hydrostatic term $(k/\eta_{\mathrm{fluid}})\rho_{\mathrm{fluid}}g\hat{\mathbf{x}}_3$, that is equal to zero in the case of vertical fault considered in this work, ζ being perpendicular to the x_3 axis; see Figure 1b.) The volumetric flow rate q_ζ has the dimension of a velocity (and therefore it is also named Darcy's velocity) and expresses the average velocity per unit area and not the fluid particle velocity.

[55] In this appendix we derive constitutive equations for fluids that relate the fluid pressure changes to the temperature changes and the heat generated on a fault. *McKenzie and Brune* [1972] and *Richards* [1976] consider the frictional heating of a planar fault with zero width; *Delaney* [1982] investigated the fluid flow and the pressurization in country rocks due to a rapid magmatic intrusion; *Lee and Delaney* [1987] solved the 1-D temperature-driven fluid pressure equation for zero thickness fault and with different unit sources.

[56] Continuity equations for pore fluid and solid (rock) mass in Eulerian formulation imply that

$$\frac{\partial}{\partial t}m_{\mathrm{fluid}}+\frac{\partial}{\partial\zeta}\left(\rho_{\mathrm{fluid}}\,q_\zeta\right)=0 \tag{B2}$$

where m_{fluid} is the fluid mass content [*Batchelor*, 1967], i.e., the fluid mass per unit volume of dry skeleton), and ρ_{fluid} is the pore fluid cubic mass density.

[57] As its rate is expressed as

$$\frac{\partial}{\partial t} m_{\text{fluid}} = \rho_{\text{fluid}} \frac{\partial}{\partial t}\Phi + \Phi \frac{\partial}{\partial t}\rho_{\text{fluid}}$$

assuming that permeability k, density ρ_{fluid} and dynamic viscosity η_{fluid} are independent on the position (i.e., spatially homogeneous), from equations (B1) and (B2) we have

$$\rho_{\text{fluid}} \frac{\partial}{\partial t}\Phi + \Phi \frac{\partial}{\partial t}\rho_{\text{fluid}} = \frac{k\rho_{\text{fluid}}}{\eta_{\text{fluid}}} \frac{\partial^2}{\partial \zeta^2} p_{\text{fluid}} \tag{B3}$$

The fluid density $\rho_{\text{fluid}}(p_{\text{fluid}}, T)$ is related to fluid pressure and temperature through the definition [see, e.g., *Batchelor*, 1967] of the coefficient of compressibility of the fluid (i.e., the inverse of the bulk modulus of elasticity of the fluid,

$$\beta_{\text{fluid}} = \frac{1}{\rho_{\text{fluid}}} \frac{\partial \rho_{\text{fluid}}}{\partial p_{\text{fluid}}}\bigg|_T$$

where the partial derivative is made in isothermal conditions) and the coefficient of thermal expansion of the fluid:

$$\alpha_{\text{fluid}} = -\frac{1}{\rho_{\text{fluid}}} \frac{\partial \rho_{\text{fluid}}}{\partial T}\bigg|_{p_{\text{fluid}}}$$

where the partial derivative is made in isobaric conditions:

$$\frac{1}{\rho_{\text{fluid}}} \frac{\partial}{\partial t}\rho_{\text{fluid}} = \beta_{\text{fluid}} \frac{\partial}{\partial t} p_{\text{fluid}} - \alpha_{\text{fluid}} \frac{\partial}{\partial t} T \tag{B4}$$

[see also *Lee and Delaney*, 1987]. From equations (B3) and (B4) we have

$$\frac{\partial}{\partial t} p_{\text{fluid}} = \frac{\alpha_{\text{fluid}}}{\beta_{\text{fluid}}} \frac{\partial}{\partial t} T - \frac{1}{\beta_{\text{fluid}}\Phi} \frac{\partial}{\partial t}\Phi + \omega \frac{\partial^2}{\partial \zeta^2} p_{\text{fluid}} \tag{B5}$$

where ω is the hydraulic diffusivity (see equation (8)).

[58] Let us assume that porosity Φ is constant in time ($\Phi(\xi_1, \zeta, \xi_3, t) = \Phi_0(\xi_1, \zeta, \xi_3)$). Under this assumption, equation (B5) becomes

$$\frac{\partial}{\partial t} p_{\text{fluid}} - \frac{\alpha_{\text{fluid}}}{\beta_{\text{fluid}}} \frac{\partial}{\partial t} T = \omega \frac{\partial^2}{\partial \zeta^2} p_{\text{fluid}} \tag{B6}$$

where the hydraulic diffusivity ω is constant over time, since porosity and permeability are constant. For an elementary heat source (see Appendix A), taking into account the solution (A1) for the temperature, the solution of equation (B6) coupled with equation (5) is

$$p^{el}_{\text{fluid}}(\zeta, t) = \frac{\gamma h}{2\sqrt{\pi t}} \left[-\frac{\sqrt{\chi}}{\omega - \chi} e^{-\frac{\zeta^2}{4\chi t}} + \frac{\sqrt{\omega}}{\omega - \chi} e^{-\frac{\zeta^2}{4\omega t}} \right] \tag{B7}$$

where the dimensionless parameter γ is $\alpha_{\text{fluid}}/(\beta_{\text{fluid}} c)$. If the heat source is expressed as in equation (A2), we obtain the solution for pressure to the simplified 1-D thermal pressurization problem (i.e., of the coupled equations (5) and (B6)) integrating over the normal coordinate ζ the temporal convolution between the Green kernel corresponding to (B7) and the actual heat source (A2):

$$\begin{aligned} p^{w}_{\text{fluid}}(\xi_1, \zeta, \xi_3, t) = p_{\text{fluid}_0} + \frac{\gamma}{4w(\xi_1, \xi_3)} \int_0^{t-\varepsilon} dt' \\ \cdot \left\{ -\frac{\chi}{\omega - \chi} \left[\text{erf}\left(\frac{\zeta + w(\xi_1, \xi_3)}{2\sqrt{\chi(t - t')}} \right) - \text{erf}\left(\frac{\zeta - w(\xi_1, \xi_3)}{2\sqrt{\chi(t - t')}} \right) \right] \right. \\ \left. + \frac{\omega}{\omega - \chi} \left[\text{erf}\left(\frac{\zeta + w(\xi_1, \xi_3)}{2\sqrt{\omega(t - t')}} \right) - \text{erf}\left(\frac{\zeta - w(\xi_1, \xi_3)}{2\sqrt{\omega(t - t')}} \right) \right] \right\} \\ \cdot \tau(\xi_1, \xi_3, t') v(\xi_1, \xi_3, t') \end{aligned} \tag{B8}$$

where p_{fluid_0} is the initial fluid pressure distribution (i.e., $p_{\text{fluid}_0} \equiv p_{\text{fluid}}(\xi_1, \zeta, \xi_3, 0)$) and we have assumed that the dimensionless parameter γ is constant over the slipping zone $2w$. As in equation (B7), in (B8) terms containing χ account for thermal contribution and terms containing ω for hydraulic one.

[59] On the fault plane (i.e., in the limit of $\zeta \to 0$) the solution for the fluid pressure is

$$\begin{aligned} p^{wf}_{\text{fluid}}(\xi_1, \xi_3, t) = p^{f}_{\text{fluid}_0} + \frac{\gamma}{2w(\xi_1, \xi_3)} \\ \cdot \int_0^{t-\varepsilon} dt' \left\{ -\frac{\chi}{\omega - \chi} \text{erf}\left(\frac{w(\xi_1, \xi_3)}{2\sqrt{\chi(t - t')}} \right) \right. \\ \left. + \frac{\omega}{\omega - \chi} \text{erf}\left(\frac{w(\xi_1, \xi_3)}{2\sqrt{\omega(t - t')}} \right) \right\} \tau(\xi_1, \xi_3, t') v(\xi_1, \xi_3, t') \end{aligned} \tag{B9}$$

where $p^{f}_{\text{fluid}_0}$ is the initial fluid pressure distribution on the fault plane (i.e., $p^{f}_{\text{fluid}_0} \equiv p_{\text{fluid}}(\xi_1, 0, \xi_3, 0)$). Also in this case it is interesting to calculate the fluid pressure response in the limit of zero thickness slipping zone:

$$\begin{aligned} p^{0f}_{\text{fluid}}(\xi_1, \xi_3, t) = p^{f}_{\text{fluid}_0} + \frac{\gamma}{2\sqrt{\pi}} \int_0^{t-\varepsilon} dt' \left\{ -\frac{\chi}{\omega - \chi} \frac{1}{\sqrt{\chi(t - t')}} \right. \\ \left. + \frac{\omega}{\omega - \chi} \frac{1}{\sqrt{\omega(t - t')}} \right\} \tau(\xi_1, \xi_3, t') v(\xi_1, \xi_3, t') \end{aligned} \tag{B10}$$

that represents the upper boundary of the fluid pressure distribution on the fault plane.

[60] We emphasize that our solution is different from that proposed by *Andrews* [2002, equation (17)] because we consider appropriate heat source and Green's kernels. *Andrews* [2002] used a Gaussian analytical expression for the elementary heat source and neglected the term involving thermal diffusivity. Moreover, there is one important advantage in our solution: due to the analytical properties of the proper Green's kernel used in this work we can limit the domain of the integration of the temporal convolution that gives p^{wf}_{fluid} up to $t - \varepsilon$. In this case, pore fluid pressure can be determined independently on the actual values (i.e., at time t) of the fault friction and fault slip velocity. Finally, we do not include any artificial fading memory in the calculation of the value of the effective normal stress at the actual time t.

[61] **Acknowledgments.** We would like to thank Joe Andrews and Paul Spudich for the discussions on the thermal pressurization effects and the heat production mechanisms during earthquakes. We are indebted to Paul Spudich for a preliminary revision of the text. We thank the Associate

Editor Douglas Toomey and two anonymous reviewers for their detailed and stimulating comments. We also thank Jim Rice for providing material in advance of publication. Finally, we are grateful to Enzo Boschi, who lively encouraged this research.

References

Allen, A. R. (1979), Mechanism of frictional fusion in fault zones, *J. Struct. Geol.*, *1*, 231–243.

Andrews, D. J. (1976a), Rupture propagation with finite stress in antiplane strain, *J. Geophys. Res.*, *81*, 3575–3582.

Andrews, D. J. (1976b), Rupture velocity of plane strain shear cracks, *J. Geophys. Res.*, *81*, 5679–5687.

Andrews, D. J. (1999), Test of two methods for faulting in finite-difference calculations, *Bull. Seismol. Soc. Am.*, *89*, 931–937.

Andrews, D. J. (2002), A fault constitutive relation accounting for thermal pressurization of pore fluid, *J. Geophys. Res.*, *107*(B12), 2363, doi:10.1029/2002JB001942.

Andrews, D. J., and Y. Ben-Zion (1997), Wrinkle-like slip pulse on a fault between different materials, *J. Geophys. Res.*, *102*, 553–571.

Antonioli, A., M. E. Belardinelli, A. Bizzarri, and K. S. Vogfjord (2006), Evidence of instantaneous dynamic triggering during the seismic sequence of year 2000 in south Iceland, *J. Geophys. Res.*, *111*, B03302, doi:10.1029/2005JB003935.

Archuleta, R. J., and S. M. Day (1980), Dynamic rupture in a layered medium: The 1996 Parkfield earthquake, *Bull. Seismol. Soc. Am.*, *70*, 671–689.

Batchelor, G. H. (1967), *An Introduction to Fluid Dynamics*, 615 pp., Cambridge Univ. Press, New York.

Beeler, N. M., and T. E. Tullis (1997), The role of time and displacement in velocity-dependent volumetric strain of fault zones, *J. Geophys. Res.*, *102*, 22,595–22,609.

Beeler, N. M., T. E. Tullis, and J. D. Weeks (1994), The roles of time and displacement in the evolution effect in rock friction, *Geophys. Res. Lett.*, *21*, 1987–1990.

Berry, F. A. F. (1973), High fluid potentials in the California Coast Range and their tectonic significance, *Am. Assoc. Pet. Geol. Bull.*, *57*, 1219–1249.

Bizzarri, A., and M. Cocco (2003), Slip-weakening behavior during the propagation of dynamic ruptures obeying rate- and state-dependent friction laws, *J. Geophys. Res.*, *108*(B8), 2373, doi:10.1029/2002JB002198.

Bizzarri, A., and M. Cocco (2005), 3-D dynamic simulations of spontaneous rupture propagation governed by different constitutive laws with rake rotation allowed, *Ann. Geophys.*, *48*, 277–299.

Bizzarri, A., and M. Cocco (2006), A thermal pressurization model for the spontaneous dynamic rupture propagation on a three-dimensional fault: 2. Traction evolution and dynamic parameters, *J. Geophys. Res.*, *111*, B05304, doi:10.1029/2005JB003864.

Bizzarri, A., M. Cocco, D. J. Andrews, and E. Boschi (2001), Solving the dynamic rupture problem with different numerical approaches and constitutive laws, *Geophys. J. Int.*, *144*, 656–678.

Blanpied, M. L., D. A. Lockner, and J. D. Byerlee (1992), An earthquake mechanism based on rapid sealing of faults, *Nature*, *358*, 574–576.

Brodsky, E. E., and H. Kanamori (2001), Elastohydrodynamic lubrication of faults, *J. Geophys. Res.*, *106*, No. B8, 16,357–16,374.

Byerlee, J. (1990), Friction, overpressure and fault normal compression, *Geophys. Res. Lett.*, *17*, 2109–2112.

Cardwell, R. K., D. S. Chinn, G. F. Moore, and D. L. Turcotte (1978), Frictional heating on a fault zone with finite thickness, *Geophys J. R. Astron. Soc.*, *52*, 525–530.

Carslaw, H. S., and J. C. Jaeger (1959), *Conduction of Heat in Solids*, 510 pp., Oxford Univ. Press, New York.

Chester, F. M. (1995), A rheologic model for wet crust applied to strike-slip faults, *J. Geophys. Res.*, *100*, 13,033–13,044.

Chester, F. M., and J. S. Chester (1998), Ultracataclasite structure and friction processes of the Punchbowl fault, San Andreas system, California, *Tectonophysics*, *295*, 199–221.

Chester, F. M., J. P. Evans, and R. L. Biegel (1993), Internal structure and weakening mechanism of the San Andreas Fault, *J. Geophys. Res.*, *98*, 771–786.

Cocco, M., and A. Bizzarri (2002), On the slip-weakening behavior of rate- and state dependent constitutive laws, *Geophys. Res. Lett.*, *29*(11), 1516, doi:10.1029/2001GL013999.

Collettini, C., L. Chiaraluce, F. Pucci, M. R. Barchi, and M. Cocco (2005), Looking at fault reactivation matching structural geology and seismological data, *J. Struct. Geol.*, *27*, 937–942, doi:10.1016/j.jsg.2004.10.016.

Darcy, H. (1856), *Les Fontaines Publiques de la Ville de Dijon*, 590 pp., Dalmont, Paris.

Das, S., and K. Aki (1977a), A numerical study of two-dimensional spontaneous rupture propagation, *Geophys. J. R. Astron. Soc.*, *50*, 643–668.

Das, S., and K. Aki (1977b), Fault plane with barriers: A versatile earthquake model, *J. Geophys. Res.*, *82*, 5658–5670.

Day, S. M. (1977), Finite element analysis of seismic scattering problems, Ph.D. thesis, Univ. of Calif., San Diego.

Day, S. M. (1982a), Three-dimensional finite difference simulation of fault dynamics: Rectangular faults with fixed rupture velocity, *Bull. Seismol. Soc. Am.*, *72*, 705–727.

Day, S. M. (1982b), Three-dimensional finite difference simulation of spontaneous rupture: The effect of nonuniform prestress, *Bull. Seismol. Soc. Am.*, *72*, 1881–1902.

Delaney, P. T. (1982), Rapid intrusion of magma into wet rocks: Groundwater flow due to pore pressure increases, *J. Geophys. Res.*, *87*, 7739–7756.

Dieterich, J. H. (1978), Time-dependent friction and the mechanics of stick slip, *Pure Appl. Geophys.*, *116*, 790–806.

Dieterich, J. H. (1986), A model for the nucleation of earthquake slip, in *Earthquake Source Mechanics*, *Geophys. Monogr. Ser.*, vol. 37, edited by S. Das, J. Boatwright, and H. Scholz, pp. 37–47, AGU, Washington, D. C.

Dieterich, J. H. (1994), A constitutive law for rate of earthquake production and its application to earthquake clustering, *J. Geophys. Res.*, *99*, 2601–2618.

Dieterich, J. H., and M. F. Linker (1992), Fault instability under conditions of variable normal stress, *Geophys. Res. Lett.*, *19*, 1691–1694.

Di Toro, G., and G. Pennacchioni (2004), Superheated friction-induced melts in zoned pseudotachylytes within the Adamello tonalities (Italian southern Alps), *J. Struct. Geol.*, *26*, 1783–1801.

Di Toro, G., D. L. Golbsby, and T. E. Tullis (2004), Friction falls toward zero in quartz rock as slip velocity approaches seismic rates, *Nature*, *427*, 436–439.

Di Toro, G., G. Pennacchioni, and G. Teza (2005), Can pseudotachylytes be used to infer earthquake source parameters? An example of limitations in the study of exhumed faults, *Tectonophysics*, *402*, 3–20.

Fialko, Y. (2004), Temperature fields generated by the elastodynamic propagation of shear cracks in the Earth, *J. Geophys. Res.*, *109*, B01303, doi:10.1029/2003JB002497.

Fialko, Y. A., and A. M. Rubin (1998), Thermodynamics of lateral dike propagation: Implications for crustal accretion at slow spreading mid-ocean ridges, *J. Geophys. Res.*, *103*, 2501–2514.

Friedman, M., J. M. Logan, and J. A. Rigert (1974), Glass-indurated quartz gouge in sliding-friction experiments on sandstone, *Geol. Soc. Am. Bull.*, *85*, 937–942.

Harris, R. A., and S. M. Day (1997), Effects of a low–velocity zone on a dynamic rupture, *Bull. Seismol. Soc. Am.*, *87*, 1267–1280.

Hobbs, B. E., and B. H. G. Brady (1985), Normal stress changes and the constitutive law for rock friction (abstract), *Eos. Trans. AGU*, *66*, 382.

Hubbert, M. K., and W. W. Rubey (1959), Mechanics of fluid-filled porous solids and its application to overthrust faulting, *Geol. Soc. Am. Bull.*, *70*, 115–166.

Ida, Y. (1972), Cohesive force across the tip of a longitudinal–shear crack and Griffith's specific surface energy, *J. Geophys. Res.*, *77*, 3796–3805.

Irwin, W. P., and I. Barnes (1975), Effect of geologic structure and metamorphic fluids on seismic behavior of the San Andreas fault system in central and northern California, *Geology*, *3*, 713–716.

Ito, H., H. Naka, D. Lockner, T. Kiguchi, H. Tanaka, R. Ikeda, T. Ohtani, K. Fujimoto, and Y. Kuwahara (1998), Permeability of the Nojima fault: Comparison of borehole results with core measurements, paper presented at 1998 Fall Meeting, Seismol. Soc. of Jpn., Tokyo.

Jeffreys, H. (1942), On the mechanics of faulting, *Geol. Mag.*, *79*, 291–295.

Kanamori, H., and E. E. Brodsky (2001), The physics of earthquakes, *Phys. Today*, *54*, 34–39.

Kanamori, H., and T. H. Heaton (2000), Microscopic and macroscopic physics of earthquakes, *GeoComplexity and the Physics of Earthquakes*, *Geophys. Monogr. Ser.*, vol. 120, edited by J. B. Rundle, D. L. Turcotte, and W. Klein, pp. 147–163, AGU, Washington, D. C.

Lachenbruch, A. H. (1980), Frictional heating, fluid pressure, and the resistance to fault motion, *J. Geophys. Res.*, *85*, 6097–6122.

Lee, T.-C., and P. Delaney (1987), Frictional heating and pore pressure rise due to fault slip, *Geophys. J. R. Astron. Soc.*, *88*, 569–591.

Li, Y. G., J. Vidale, K. Aki, C. Marone, and W. K. Lee (1994), Fine structure of the Landers fault zone: Segmentation and the rupture process, *Science*, *265*, 367–380.

Linker, M. F., and J. H. Dieterich (1992), Effects of variable normal stress on rock friction: Observations and constitutive equations, *J. Geophys. Res.*, *97*, 4923–4940.

Lockner, D., and J. Byerlee (1995), An earthquake instability model based on fault containing high fluid-pressure compartments, *Pure Appl. Geophys.*, *145*, 717–745.

Lockner, D., R. Summers, and J. Byerlee (1986), Effects of temperature and sliding rate of frictional strength of granite, *Pure Appl. Geophys.*, *124*, 445–469.

Lockner, D., H. Naka, H. Tanaka, H. Ito, and R. Ikeda (2000), Permeability and strength of the Nojima core samples from the Nojima fault of the 1995 Kobe earthquake, in *Proceedings of the International Workshop on*

the Nojima Fault Core and Borehole Data Analysis Nov 22–23, 1999, edited by H. Ito et al., *U.S. Geol. Surv. Open File Rep., 00-129*, 147–152.
Madariaga, R., and K. B. Olsen (2000), Criticality of rupture in 3-D, *Pure Appl. Geophys.*, *157*, 1981–2001.
Mair, K., and C. Marone (2000), Shear heating in granular layers, *Pure Appl. Geophys.*, *157*, 1847–1866.
Marone, C. (1998), Laboratory-derived friction laws and their application to seismic faulting, *Annu. Rev. Earth Planet. Sci.*, *26*, 643–696.
Mase, C. W., and L. Smith (1985), Pore-fluid pressures and frictional heating on a fault surface, *Pure Appl. Geophys.*, *92*, 6249–6272.
Mase, C. W., and L. Smith (1987), Effects of frictional heating on the thermal, hydrologic, and mechanical response of a fault, *J. Geophys. Res.*, *92*, 6249–6272.
McKenzie, D., and J. N. Brune (1972), Melting on fault planes during large earthquakes, *Geophys. J. R. Astron. Soc.*, *29*, 65–78.
Melosh, H. J. (1979), Acoustic fluidization: A new geologic process?, *Geophys. Res.*, *84*, 7513–7520.
Melosh, H. J. (1996), Dynamic weakening of faults by acoustic fluidization, *Nature*, *397*, 601–606.
Miller, S. A. (2002), Properties of large ruptures and the dynamical influence of fluids on earthquakes and faulting, *J. Geophys. Res.*, *107*(B9), 2182, doi:10.1029/2000JB000032.
Miller, S. A., A. Nur, and D. L. Olgaard (1996), Earthquakes as a coupled shear stress–high pore pressure dynamical system, *Geophys. Res. Lett.*, *23*, 197–200.
Miller, S. A., C. Collettini, L. Chiaraluce, M. Cocco, M. R. Barchi, and B. J. P. Kaus (2004), Aftershocks driver by high-pressure CO_2 source at depth, *Nature*, *427*, 724–727.
Mizoguchi, K., T. Hirose, and T. Shimamoto (2000), Permeability structure of Nojima fault: Analysis of Funaki outcrop in Hohundan, Tsuna-gun, Hyogo Prefecture (in Japanese), *Earth Mon. Extra*, *31*, 58–65.
Morrow, C. A., L. Q. Shi, and J. D. Byerlee (1984), Permeability of fault gouge under confining pressure and shear stress, *J. Geophys. Res.*, *89*, 3193–3200.
Morse, P., and H. Feshbach (1953), *Methods of Theoretical Physics*, 997 pp., McGraw-Hill, New York.
Nur, A., and J. Booker (1972), Aftershocks caused by pore fluid flow?, *Science*, *175*, 885–887.
Ohnaka, M. (2003), A constitutive scaling law and a unified comprehension for frictional slip failure, shear fracture of intact rock, and earthquake rupture, *J. Geophys. Res.*, *108*(B2), 2080, doi:10.1029/2000JB000123.
Okubo, P. G. (1989), Dynamic rupture modeling with laboratory–derived constitutive relations, *J. Geophys. Res.*, *94*, 12,321–12,335.
Olsson, W. A. (1988), The effect of normal stress history on rock friction, in *Key Questions in Rock Mechanics: Proceedings of the 29th U. S. Symposium*, edited by P. A. Cundall, R. L. Sterling, and A. M. Starfield, pp. 111–117, A. A. Balkema, Brookfield, Vt.
Otsuki, K., N. Monzawa, and T. Nagase (2003), Fluidization and melting of fault gouge during seismic slip: Identification in the Nojima fault zone and implications for focal earthquake mechanisms, *J. Geophys. Res.*, *108*(B4), 2192, doi:10.1029/2001JB001711.
Perfettini, H., R. S. Stein, R. Simpson, and M. Cocco (1999), Stress transfer by the 1988–1989 $M = 5.3$ and 5.4 Lake Elsman foreshocks to the Loma Prieta fault: Unclamping at the site of peak mainshock slip, *J. Geophys. Res.*, *104*, 20,169–20,182.
Perfettini, H., J. Schmittbuhl, and A. Cochard (2003), Shear and normal load perturbations on a two-dimensional continuous fault: 2. Dynamic triggering, *J. Geophys. Res.*, *108*(B9), 2409, doi:10.1029/2002JB001805.
Prakash, V. (1998), Frictional response of sliding interfaces subjected to time varying normal pressure, *J. Tribol.*, *120*, 97–102.
Raleigh, C. B., and J. Everden (1981), Case for low deviatoric stress in the lithosphere, in *The Mechanical Behavior of Crustal Rocks*, *Geophys. Monogr. Ser.*, vol. 24, edited by N. L. Carter et al., pp. 173–186, AGU, Washington, D. C.
Rice, J. R. (1992), Fault stress states, pore pressure distributions, and the weakness of the San Andreas Fault, in *Fault Mechanics and Transport Properties in Rocks (the Brace Volume)*, edited by B. Evans and T.-F. Wong, pp. 475–503, Elsevier, New York.
Rice, J. R. (1993), Spatio-temporal complexity of slip on a fault, *J. Geophys. Res.*, *98*, 9885–9907.
Rice, J. R. (1999), Flash heating at asperity contacts and rate-dependent friction, *Eos Trans. AGU*, *81*(46), Fall Meet. Suppl., Abstract T12B-08.
Rice, J. R. (2006), Heating and weakening of faults during earthquake slip, *J. Geophys. Res.*, doi:10.1029/2005JB004006, in press.
Rice, J. R., and M. Cocco (2006), Seismic fault rheology and earthquake dynamics, in *The Dynamics of Fault Zones, 95th Dahlem Workshop (Berlin, January, 2005)*, edited by M. R. Handy, MIT Press, Cambridge, Mass., in press.
Richards, P. G. (1976), Dynamic motions near an earthquake fault: A three-dimensional solution, *Bull. Seismol. Soc. Am.*, *66*, 1–32.
Richardson, E., and C. Marone (1999), Effects of normal stress vibrations on frictional healing, *J. Geophys. Res.*, *104*, 28,859–28,878.
Roy, M., and C. Marone (1996), Earthquake nucleation on model faults with rate- and state-dependent friction: Effects of inertia, *J. Geophys. Res.*, *101*, 13,919–13,932.
Rudnicki, J. W., and C.-H. Chen (1988), Stabilization of rapid frictional slip on a weakening fault by dilatant hardening, *J. Geophys. Res.*, *93*, 4745–4757.
Ruina, A. L. (1980), Friction laws and instabilities: A quasistatic analysis of some dry frictional behavior, Ph.D. thesis, Brown Univ., Providence, R. I.
Ruina, A. L. (1983), Slip instability and state variable friction laws, *J. Geophys. Res.*, *88*, 10,359–10,370.
Scholz, C. H. (2002), *The Mechanics of Earthquakes and Faulting*, 2nd ed., 471 pp., Cambridge Univ. Press, New York.
Segall, P., and J. R. Rice (1995), Dilatancy, compaction, and slip instability of a fluid-infiltrated fault, *J. Geophys. Res.*, *100*, 22,155–22,171.
Shapiro, S. A., R. Patzig, E. Rothert, and J. Rindshwentner (2003), Triggering of seismicity by pore-pressure perturbations: Permeability-related signature of the phenomenon, *Pure Appl. Geophys.*, *160*, 1051–1066.
Sibson, R. H. (1973), Interaction between temperature and pore-fluid pressure during earthquake faulting—A mechanism for partial or total stress relief, *Nature*, *243*, 66–68.
Sibson, R. H. (1977), Kinetic shear resistance, fluid pressures and radiation efficiency during seismic faulting, *Pure Appl. Geophys.*, *115*, 387–400.
Sibson, R. H. (1986), Brecciation processes in fault zones: Inferences from earthquake rupturing, *Pure Appl. Geophys.*, *124*, 169–175.
Sibson, R. H. (2003), Thickness of the seismic slip zone, *Bull. Seismol. Soc. Am.*, *93*, 1169–1178.
Sleep, N. H. (1995a), Frictional heating and the stability of rate and state dependent frictional sliding, *Geophys. Res. Lett.*, *22*, 2785–2788.
Sleep, N. H. (1995b), Ductile creep, compaction, and rate and state dependent friction within major fault zones, *J. Geopys. Res.*, *100*, 13,065–13,080.
Sleep, N. H. (1997), Application of a unified rate and state friction theory to the mechanics of fault zones with strain localization, *J. Geophys. Res.*, *102*, 2875–2895.
Sleep, N. H. (1999), Rate- and state-dependent friction of intact rock and gouge, *J. Geophys. Res.*, *104*, 17,847–17,855.
Sleep, N. H., and M. L. Blanpied (1992), Creep, compaction and the weak rheology of major faults, *Nature*, *359*, 687–692.
Sleep, N. H., E. Richardson, and C. Marone (2000), Physics of friction and strain rate localization in synthetic gouge, *J. Geophys. Res.*, *105*, 25,875–25,890.
Sommerfeld, A. (1950), *Mechanics of Deformable Bodies*, Elsevier, New York.
Spikes, H. (1997), Mixed lubrication—An overview, *Lubric. Sci.*, *9*, 221–253.
Spray, J. G. (1993), Viscosity determinations of some frictionally generated silicate melts: Implications for fault zone rheology at high strain rates, *J. Geophys. Res.*, *98*, 8053–8068.
Stefan, J. (1891), Uber die theorie der eisbildung, insbesondere die eisbildung im polarmene, *Ann. Phys. Chem.*, *42*, 269–286.
Terzaghi, K., R. B. Peck, and G. Mesri (1996), *Soil Mechanics in Engineering Practice*, 3rd ed., John Wiley, Hoboken, N. J.
Teufel, L. W., and J. M. Logan (1979), Effect of displacement rate on the real area of contact and temperatures generated during frictional sliding of Tennessee sandstone, *Pure Appl. Geophys.*, *116*, 840–865.
Tinti, E., A. Bizzarri, A. Piatanesi, and M. Cocco (2004), Estimates of slip weakening distance for different dynamic rupture models, *Geophys. Res. Lett.*, *31*, L02611, doi:10.1029/2003GL018811.
Tinti, E., P. Spudich, and M. Cocco (2005), Earthquake fracture energy inferred from kinematic rupture models on extended faults, *J. Geophys. Res.*, *110*, B12303, doi:10.1029/2005JB003644.
Tsutsumi, A., and T. Shimamoto (1997), High velocity frictional properties of gabbro, *Geophys. Res. Lett.*, *24*, 699–702.
Turcotte, D. L., and G. Schubert (2002), *Geodynamics*, 2nd ed., 456 pp., Cambridge Univ. Press, New York.
Wang, H. F. (2000), *Theory of Linear Poroelasticity*, 287 pp., Princeton Univ. Press, Princeton, N. J.
Wang, W., and C. H. Scholz (1983), Micromechanics of the velocity and normal stress dependence of rock friction, *Pure Appl. Geophys.*, *143*, 303–315.
Wibberley, C. A. J., and T. Shimamoto (2003), Internal structure and permeability of major strike-slip fault zones: The Median Tectonic Line in mid prefecture, southwest Japan, *J. Struct. Geol.*, *25*, 59–78.
Yamashita, T. (1998), Simulation of seismicity due to fluid migration in a fault zone, *Geophys. J. Int.*, *132*, 661–675.

A. Bizzarri, Istituto Nazionale di Geofisica e Vulcanologia, Sezione di Bologna, Via Donato Creti, 12, I-40128, Bologna, Italy. (bizzarri@bo.ingv.it)
M. Cocco, Istituto Nazionale di Geofisica e Vulcanologia, Sezione di Sismologia e Tettonofisica, Via di Vigna Murata, 605, I-00143, Rome, Italy.